Final Report

Project Title:	**FRACTAL NANOSTRUCTURED SOLAR SELECTIVE SURFACES FOR NEXT GEN CONCENTRATING SOLAR POWER**
Project Period:	08/01/2019–02/29/2024
Budget Period:	08/01/2019–02/29/2024
Submission Date:	05/31/2024
Recipient:	Virginia Polytechnic Institute & State University
Address:	*Advanced Materials and Technologies Laboratory* Virginia Tech Department of Mechanical Engineering 445 Goodwin Hall, 635 Prices Fork Road - MC 0238 Blacksburg, VA 24061
Website (if available)	**https://amtl.me.vt.edu/**
Award Number:	DE-EE0008537
Project Team:	Virginia Polytechnic Institute & State University
Principal Investigator:	Professor Ranga Pitchumani Phone: (540) 231-7183 Email: pitchu@vt.edu
Business Contact:	Nevada Davis Phone: (540) 231-1427 Email: ngdean@vt.edu
HQ Tech Manager:	Matthew Bauer
HQ Project Officer:	Christine Carter
GO Grant Specialist:	Elizabeth Parrish
GO Contracting Officer:	Pamela Brodie

ACKNOWLEDGMENT AND DISCLAIMER

Acknowledgement: This material is based upon work supported by the U.S. Department of Energy's Office of Energy Efficiency and Renewable Energy (EERE) under the Solar Energy Technologies Office (SETO) award number DE-EE0008537.

Major Goals & Objectives:

The overall goal of this project is to identify successful coating, process parameter and receiver design that demonstrate LCOC < 0.055$/MWht and degradation rate < 0.5%/year at 750°C and receiver cost < $150/kWt. (SETO target). This goal will be achieved by developing fractal-textured solar selective surfaces on high temperature stable substrates by electrodeposition and other cost effective deposition methods, with high absorptance in the solar spectrum (0.3–2.5 μm) and low emittance in the IR spectrum (~2–20 μm), resulting in a high figure of merit (FOM), low Levelized Cost of Coating (LCOC), and long-term air stability in the temperature range of 750–800oC. Specifically, we aim to demonstrate solar selective surfaces with the following attributes:

a. high thermal efficiency (>93%);
b. excellent durability (thermal endurance > 95%) at high temperatures (>750°C) in air subjected to isothermal and cyclic thermal conditions.
c. levelized cost of coating (LCOC) < 0.055$/MWht at 750°C, which is better than the current LCOC for Pyromark 2500 at 565°C;
d. projected lifetime greater than 10,000 cycles, with reapplications at appropriate intervals.

Main Project Objectives:

A statistically designed experiment matrix that contains the list of substrates and coatings to be tested will be developed based on a comprehensive literature review. We will demonstrate the capability to electrodeposit aggressively textured surfaces with fractal dimensions > 1.5 for various substrates (Inconel and Haynes) and characterize fractal dimension as a function of electrodeposition potential. Optical properties of the samples namely, solar absorptance and thermal emittance, will be measured to calculate the figure of merit (FOM) and we will demonstrate higher FOM coating than the benchmark (93%) set by previous DOE projects by means of fractal texturing of the substrate. We will evaluate the mechanical durability of the coatings using several standardized tests such as sand abrasion (ASTM D968), adhesion (ASTM D3359), and water resistance (ASTM D870) to fully characterize and demonstrate the durability of the fabricated surfaces. For samples meeting or exceeding the foregoing criteria, extensive testing of the high temperature endurance of the solar absorber coating will be conducted by subjecting them through isothermal testing at 750°C for 100 h and 750 h, and cyclic temperature of 750°C to room temperature for 50 cycles in an air environment. The FOM and mechanical durability endurance of the samples subjected to thermal testing will be tested and compared with the metric calculated prior to thermal testing. Further, the coatings fractal textured morphology will be developed on cylindrical surfaces and demonstrated to be durable and with high FOM exceeding 93%. The coatings will be subject to thermal endurance testing (750°C) for 100 h and 1000 h, as well as thermal cyclic testing (between room temperature and 750°C) for 10 and 50 thermal cycles. The durability and FOM of the coatings will be systematically demonstrated. A technoeconomic model will be developed to elucidate the combined cost/performance benefit of the coatings for Gen3 application environments in various geographical locations and DNI conditions.

The tasks and their completions are summarized in the Project Milestone Table, Table 1, which shows successful demonstrations of all the milestones, as discussed in the identified sections, figures, and tables of the report.

Table 1: Milestone Table for the Project

Task No.	Description	Success Value and Assessment Tool		Goal Met (Y/N)
Budget Period 1				
T-1	**Fabrication and Characterization of Solar Selective Surfaces**			
ST-1.1	Literature review to identify feasible material to generate fractal solar selective surfaces using electrodeposition			Y
M (ST-1.1)	Development of experimental design matrix which incorporates all the factors including choice of substrate, coating material and electrodeposition process conditions.	DOE Matrix	Sec. A.2	Y
ST-1.2	Fabrication of multiscale fractal textured surfaces on a range of materials			Y
ST-1.3	SEM, XRD, EDS and power spectra characterization of the samples and evaluation of fractal dimensions			Y
M (ST-1.3)	Demonstrate fractal dimension > 1.5, of which at least 10 replicates for each combination identified in the design of experiment matrix are suitable for FOM testing	Fractal dimensions One tailed Student t-test at 95% confidence level	Sec. A.4	Y
T-2	**Optical and Mechanical Characterization of SSC**			
ST-2.1	Optical characterization to calculate FOM at concentration ratio of 1000 suns and 750°C			Y
M (ST-2.1)	Demonstrate FOM > 0.93 at concentration ratio of 1000 suns and temperature of 750°C demonstrated at least on ten replicates that will be used for isothermal and thermal cycling endurance testing.	• One-tailed Student t-test at 95% confidence level • FOM measured mean > FOM success value.	Sec. B.2	Y
ST-2.2	Mechanical durability testing using the ASTM protocols			
G/NG-1	Demonstrate FOM > 0.93, Adhesion strength > 0.95, Mechanical durability endurance > 0.95, and	• FOM, • Adhesion Strength based on ASTM D3359,	Sec. B	Y

	Water durability endurance > 0.95 for at least 10 replicates that will be used for isothermal and thermal cycling endurance testing in Budget Period 2.	• Mechanical durability endurance based on sand abrasion ASTM D968, • Water durability endurance based on ASTM D870		
Budget Period 2				
T-3	**Thermal Endurance Characterization of SSC**			
ST-3.1	Isothermal testing of the samples			Y
ST-3.2	FOM and Mechanical durability characterization of the samples subjected to isothermal testing			Y
M (ST-3.2) 100 h, 750°C	Demonstrate: 1. Isothermal endurance = FOM [t=100 h,750°C]/FOM [t=0 h,750°C] > 0.95 2. Adhesion strength based on ASTM D3359 = (Total Area [t=100 h,750 C] – Area Lost)/Total Area [t=100 h,750°C] > 0.95 3. Mechanical durability endurance: FOM after durability testing [t=100 h,750°C]/FOM before durability testing [t=100 h,750°C] > 0.95 4. Water durability endurance: FOM after durability testing [t=100 h,750°C]/FOM before durability testing [t=100 h,750°C] > 0.95 5. Water quenching endurance: FOM before quenching [t=100 h,750°C]/FOM after quenching [t=100 h,750°C] > 0.95	Isothermal endurance at 750°C for 100 hours Isothermal endurance Adhesion Strength based on ASTM D3359 Mechanical durability endurance based on sand abrasion ASTM D968 Water durability endurance based on ASTM D870 Water quenching test from 750°C	Sec. C.1	Y
M (ST-3.3) 750 h, 750°C	Demonstrate: 1. Isothermal endurance = FOM [t=750 h,750°C]/ FOM [t=0 h,750°C] > 0.95 2. Adhesion strength based on ASTM D3359 = (Total Area	Isothermal endurance at 750°C for 750 hours Isothermal endurance	Sec. C.2	Y

	[t=750 h,750°C] – Area Lost)/Total Area [t=750 h,750°C] > 0.95 3. Mechanical durability endurance: FOM after durability testing [t=750 h,750°C]/FOM before durability testing [t=750 h,750°C] > 0.95 4. Water durability endurance: FOM after durability testing [t=750 h,750°C]/FOM before durability testing [t=750 h,750°C] > 0.95 5. Water quenching endurance: FOM before quenching [t=750 h,750°C]/FOM after quenching [t=750 h,750°C] > 0.95	Adhesion Strength based on ASTM D3359 Mechanical durability endurance based on sand abrasion ASTM D968 Water durability endurance based on ASTM D870 Water quenching test from 750°C		
ST-3.3	Thermal cyclic testing of samples			Y
ST-3.4	FOM, Mechanical durability and Mechanical durability characterization of the samples subjected to thermal cyclic testing			Y
M(ST-3.4) <u>50 cycles, 750°C</u>	Demonstrate: 1. Thermal cycling endurance = FOM [50 cycles,750°C]/FOM [0 cycles,750°C] > 0.95 2. Adhesion strength based on ASTM D3359 = (Total Area [50 cycles,750°C] – Area Lost)/Total Area [50 cycles,750°C] > 0.95 3. Mechanical durability endurance: FOM after durability testing [50 cycles,750°C]/FOM before durability testing [50 cycles,750°C] > 0.95 4. Water durability endurance: FOM after durability testing [50 cycles,750°C]/FOM before durability testing [50 cycles,750°C] > 0.95 5. Water quenching endurance: FOM after quenching [50	<u>After 50 cycles of thermal cyclic testing to 750°C</u>: Thermal cycling endurance Adhesion Strength based on ASTM D3359 Mechanical durability endurance based on sand abrasion ASTM D968 Water durability endurance based on ASTM D870 Water quenching test from 750°C	Sec. C.3	Y

	cylces,750°C]/FOM before quenching [50 cylces,750°C] > 0.95			
Budget Period 3				
T-4, T-5	**Technoeconomic analysis and Technology to Market Plan**			
ST-4.1	System/Cost model			Y
ST-4.2	System performance and cost investigation			Y
T-6	**Fabrication and Characterization of Solar absorber Coatings on Tubular Geometry**			
ST-6.1	Fabrication of multiscale fractal textured surfaces on a range of tubular materials			Y
ST-6.2	SEM, XRD, EDS and power spectra characterization of the tubular samples and evaluation of fractal dimensions			Y
M(ST-6)	Comparable morphology and fractal development on tubular surfaces compared to coatings for flat surfaces.	Fractal dimension	Sec. D	Y
T-7	**Optical and Mechanical Characterization of Tubular SSC**			
ST-7.1	Optical characterization to calculate Absorptance at concentration ratio of 1000 suns and temperature of 750°C			Y
M (7.1)	Demonstrate absorptance > 0.975 for 5 samples of SAC coating on the tubular surfaces. By comparing the optical characteristics, demonstrate that cylindrical surfaces have homogeneous coatings throughout the four quadrants and length of the tubes.	Absorptance	Sec. E	Y
ST-7.2	Mechanical durability, adhesion, water immersion tests of as deposited coatings on cylindrical substrates.			Y

M (7.2)	Demonstrate absorptance > 0.975, Adhesion strength > 0.95, Mechanical durability endurance > 0.95, and Water durability endurance > 0.95 for at least 5 replicates that will be used for isothermal and thermal cycling endurance testing.	Absorptance, Adhesion Strength, Mechanical durability endurance based on sand abrasion ASTM D968, Water durability endurance based on ASTM D870	Sec. E	Y
T-8	**Thermal Endurance Characterization of Tubular SSC**			
ST-8.1	Isothermal testing of tubular surfaces at 750 C for 100 hours and 1000 hours			Y
ST-8.2	Absorptance, and mechanical durability characterization of tubular surfaces subjected to isothermal testing at 750 C for 100 hours and 1000 hours			Y
M(8.1) 100 h, 750°C	Demonstrate: 1. Isothermal endurance = FOM [t=100 h,750°C]/ FOM [t=0 h,750°C] > 0.95 2. Adhesion strength based on ASTM D3359 = (Total Area [t=100 h,750 C] – Area Lost)/Total Area [t=100 h,750°C] > 0.95 3. Mechanical durability endurance: FOM after durability testing [t=100 h,750°C]/FOM before durability testing [t=100 h,750°C] > 0.95 4. Water durability endurance: FOM after durability testing [t=100 h,750°C]/FOM before durability testing [t=100 h,750°C] > 0.95 5. Water quenching endurance: FOM before quenching [t=100 h,750°C]/FOM after quenching [t=100 h,750°C] > 0.95	Isothermal endurance at 750°C for 100 hours Adhesion measure Mechanical durability endurance based on sand abrasion ASTM D968 Water durability endurance based on ASTM D870 Water quenching test from 750 C	Sec. F	Y

M(8.2) 1000 h, 750°C	Demonstrate: 1. Isothermal endurance = FOM [t=1000 h,750°C]/FOM [t=0 h,750°C] > 0.95 2. Adhesion strength based on ASTM D3359 = (Total Area [t=1000 h,750°C] – Area Lost)/Total Area [t=1000 h,750°C] > 0.95 3. Mechanical durability endurance: FOM after durability testing [t=1000 h,750°C]/FOM before durability testing [t=1000 h,750°C] > 0.95 4. Water durability endurance: FOM after durability testing [t=1000 h,750°C]/FOM before durability testing [t=1000 h,750°C] > 0.95 5. Water quenching endurance: FOM before quenching [t=1000 h,750°C]/FOM after quenching [t=1000 h,750°C] > 0.95	Isothermal endurance at 750°C <u>for 1000 hours</u> Adhesion measure Mechanical durability endurance based on sand abrasion ASTM D968 Water durability endurance based on ASTM D870 Water quenching test from 750°C	Sec. F	Y
ST-8.3	Thermal cyclic testing of absorber coating on tubular surfaces 10, and 50 cycles			Y
ST-8.4	Absorptance, Mechanical durability and Mechanical durability characterization of the tubular solar absorber surfaces subjected to thermal cyclic testing			Y
M(8.3) 10 cycles, 750°C	Demonstrate: 1. Thermal cycling endurance = Absorptance [10 cycles,750°C]/ absorptance [t=0 cycles,750°C] > 0.95 2. Adhesion strength = Absorptance after adhesion test [10 cycles,750°C]/ absorptance before adhesion test [10 cycles,750°C] > 0.95 3. Mechanical durability endurance: Absorptance after durability testing [10 cycles,750°C]/	Thermal cycling endurance at 750°C <u>for 10 cycles</u> Adhesion measure Mechanical durability endurance based on sand abrasion ASTM D968 Water durability endurance based on ASTM D870	Sec. F	Y

	absorptance before durability testing [10 cycles,750°C] > 0.95 4. Water durability endurance: Absorptance after durability testing [10 cycles,750°C]/absorptance before durability testing [10 cycles,750°C] > 0.95 5. Water Quenching endurance: Absorptance after quenching [10 cycles,750°C]/absorptance before quenching [10 cycles,750°C] > 0.95	Water quenching test from 750°C		
M(8.4) 50 cycles, 750°C	Demonstrate: 1. Thermal cycling endurance = Absorptance [50 cycles,750°C]/ absorptance [t=0 cycles,750°C] > 0.95 2. Adhesion strength = Absorptance after adhesion test [50 cycles,750°C]/ absorptance before adhesion test [50 cycles,750°C] > 0.95 3. Mechanical durability endurance: Absorptance after durability testing [50 cycles,750°C]/ absorptance before durability testing [50 cycles,750°C] > 0.95 4. Water durability endurance: Absorptance after durability testing [50 cycles,750°C]/absorptance before durability testing [50 cycles,750°C] > 0.95 5. Water quenching endurance: Absorptance after quenching [50 cycles,750°C]/absorptance before quenching [50 cycles,750°C] > 0.95	Thermal cycling endurance at 750°C <u>for 50 cycles</u> Thermal Cycling endurance Adhesion measure Mechanical durability endurance based on sand abrasion ASTM D968 Water durability endurance based on ASTM D870 Water quenching test from 750°C	Sec. F	Y
FD-1	Identify successful coating, process parameter and receiver design that demonstrate LCOC < 0.055$/MWht at 750°C (LCOC for Pyromark 2500 at 565°C)	Levelized Cost of Coating (LCOC)	Sec. G	Y

FD-2	T2M: Testing at NREL on industry relevant protocol.	Absorptance ratio after/before > 0.95		Y

PROJECT RESULTS AND DISCUSSION[1]**:**
The description in this section follows the order of the tasks in the milestone table. The relevant task/subtask/milestone numbers are highlighted in the section headings for ease of tracking.

Section A: Extensive literature review on absorber coatings at a range of temperatures to identify potential materials for the present study. Description of the development of multiscale textured morphologies on flat surfaces via electrodeposition with high fractal dimension, demonstrating completion of T-1 tasks and successful accomplishment of milestones M(ST-1.1) and M(ST-1.3).

Section B: Optical and mechanical characterization of the absorber coatings on flat surfaces demonstrating efficiency greater than 93% and mechanical durability through ASTM testing with statistical t-tests. Section B demonstrates completion of T-2 tasks, successful accomplishment of milestone M(ST-2.1), and meeting G/NG-1 targets.

Section C: Thermal endurance characterization of the fractal textured absorber coatings on flat surfaces including isothermal endurance at 750°C for up to 750 h and thermal cyclic endurance between room temperature and 750°C for up to 50 cycles. Demonstrates completion of T-3 tasks and successful accomplishment of milestones M(ST-3.2), M(ST-3.3), and M(ST-3.4).

Section D: Description of the development of multiscale textured morphologies on tubular surfaces via electrodeposition with high fractal dimension, demonstrating completion of T-6 tasks and successful accomplishment of milestone M(ST-6).

Section E: Optical and mechanical characterization of the absorber coatings on tubular surfaces demonstrating absorptance greater than 0.975 and mechanical durability through ASTM testing with statistical t-tests. Section E demonstrates completion of T-7 tasks, and successful accomplishment of milestones M(7.1) and M(7.2).

Section F: Thermal endurance characterization of the fractal textured absorber coatings on tubular surfaces including isothermal endurance at 750°C for up to 1000 h and thermal cyclic endurance between room temperature and 750°C for up to 50 cycles. Demonstrates completion of T-8 tasks and successful accomplishment of milestones M(8.1), M(8.2), M(8.3), and M(8.4).

Section G: Technoeconomic analysis in support of tasks T-4 and T-5, demonstrating successful accomplishment of FD-1 and FD-2.

Section H: Summary of findings from the project.

A. Fabrication and Characterization of Solar Absorber Surfaces — M(ST-1.1), M(ST-1.3)

[1] See EERE 355 FARC Section IA2b

A.1. ST-1.1 Literature Review

The goal of the literature review was to identify studies on air-stable coatings on thermal receivers over a range of temperatures 300 °C up to Gen3 temperatures. The study over the broad range of temperatures, and not just Gen3 temperatures, is partly motivated by the absence of a comprehensive review of the developments in air-stable coatings, in general. The studies sought to investigate materials, coating fabrication methods, optical properties and thermal endurance characteristics of the coatings. It was found that even though there is plenty of literature available for solar selective coatings in general, most are focused on vacuum or inert conditions and relatively little work is reported on thermal endurance in air and open environmental conditions seen in central receivers. In the discussion below, the coatings are considered in the following four groups: (1) Dielectric-metal-dielectric multilayer solar selective coatings, (2) Graded material coatings, (3) Cermet coatings, and (4) Oxide coatings.

A.1.1. Summary Tables

The literature review is summarized in two tables of solar absorbers of different temperature stability regimes. Table 2 shows the reported solar absorber coatings tested for stability in the temperature range of 400 °C to 600 °C in air. Similarly, Table 3 catalogs solar selective coatings stable in a higher temperature range of 600°C and above. In each Table, the available information is presented in terms of the coating and substrate materials, the deposition method, the maximum temperature stability, and parenthetically the duration for which the stability was demonstrated, as well as the measured optical properties both as-deposited and after the high-temperature testing. The data is ordered from the lowest temperature to the highest temperature of stability. For reference, the source of each data presented is also provided.

It is seen from Table 2 that many multilayer coatings deposited by sputtering, evaporation, etc., are stable up to 600°C in air. The coatings stable up to 600°C show excellent solar selectivity with high solar absorptance and low solar emittance required for solar absorber application in Gen 2 or earlier CSP systems. About an equal number of coatings in the Table are stable in the 500–600°C range and the 400–500°C range. Multilayer coatings of Al/AlN, AlxOy/Al/AlOy, TiAlN/SiCNH, CrN(H)/CrN(L)/CrON/Al2O3/, HfMoN(H)/HfMoN(L)/HfON/Al2O3, AlxOy/Pt/AlxOy, Ni-Al2O3, Mo/HfOx/Mo/HfO2, W/WAlN/WAlON/Al2O3, AlxOy/Pt/AlxOy deposited by sputtering showed good solar selectivity, i.e., solar absorptance > 90% and thermal emittance < 20%.

Table 2: Solar absorber coating stable in air at 400°C to 600°C of temperature regime.

S.No	Material	Deposition method	Substrate	Temperature (annealed in air)	Absorptance (α) (as depo. /after annealed)	Emittance (ε)	Reference
1	Al/AlN	Sputtering	Glass	400˚C	0.93	0.04	S. Zhao, E. Wackelgard, The optical properties of sputtered composite of Al–AlN, Solar Energy Materials and Solar Cells 90 (2006) 1861–1874.
2	Al_xO_y–Al–Al_xO_y	Sputtering	Copper	400˚C (2h)	0.95-0.97	0.05-0.08	H.C. Barshilia, N. Selvakumar, G. Vignesh, K.S. Rajam, A. Biswas, Optical properties and thermal stability of pulsed sputter deposited Al_xO_y/Al/Al_2O_3 multilayer absorber coatings, Solar Energy Materials and Solar Cells 93 (2009) 315–323
3	CrN(H)/CrN(L)/CrON/ Al_2O_3	DC Sputtering	Stainless steel	400˚C (2 h) in air	0.93/0.91	0.14/0.15	T.K. Tsai,Y.H. Li, J.S.Fang, Spectral properties and thermal stability of CrN/CrON/Al2O3 spectrally selective coating, Thin Solid Films 615 (2016) 91–96.
4	Co_3O_4	electrodeposition	Stainless steel	400 ˚C (10 h) in air	0.97	--	Z. Abdel Hamid, A. Abdel Aal and P. Schmuki, Surf. Interface Anal. 2008, 40, 1493–1499.
5	cobalt oxide-iron oxide coatings	spray pyrolysing aqueous	Stainless steel	400˚C (24 h) in air	0.94	0.20	C S UMA, L K MALHOTRA and K L CHOPRA, Bull. Mater. Sci., Vol. 8, No. 3, June 1986, pp. 385-389.
6	W/WAlN/WAlON/Al_2O_3	Sputtering	Stainless steel	400 ˚C (309 h) in air	0.90	$0.15_{c=100}$	Atasi Dan, et al., ACS Appl. Energy Mater. 2019, 2, 8, 5557-5567
7	Au–MgO	Sputtering	Mo coated Stainless steel	400 ˚C (64 h)	0.90	0.10 at 100 °C	D.M. Bezes, J. Valignat, Optical properties of gold–magnesia selective cermets, Solar Energy Materials 7 (1982) 203–211.
8	Ni/MgF_2	Evaporation	Nickel mirror	450˚C (470 h) in air	0.96/0.94	0.13/0.13	M. MAST, K. GINDELE AND M. KOHL, Thin Sohd Film, 126 (1985) 37-42.
9	HfMoN(H)/HfMoN(L)/ HfON/Al_2O_3	Sputtering	Stainless steel	475˚C (34 h) air 600˚C (450 h) in vacuum 650˚C (100 h) in vacuum	0.94–0.95	0.13–0.14	N. Selvakumar, N.T.Manikandanath, A. Biswas, Harish C. Barshilia, Solar Energy Materials & Solar Cells 102 (2012) 86–92.
10	Mn–Cu–Fe composite oxide	controlled thermal oxidation process	Stainless steel -J4	500˚C (>100 h) in air	0.915	0.19	A. Srinivasa Rao, S. Sakthivel, Journal of Alloys and Compounds 644 (2015) 906–915.
11	CrAlO	cathodic arc ion plating	Stainless steel	500˚C (200 h) in air	0.923	0.149	H.D. Liu, et al. Solar Energy Materials & Solar Cells 134 (2015) 261–267.
12	Ni-Al_2O_3/ Al_2O_3	Vacuum evaporation	Fused Quartz	500˚C (115 h) air	0.94	0.1	H.G. Craighead, R.A. Buhrman, Optical properties of selectively absorbing Ni/Al2O3 composite films, Applied Physics Letters 31 (1977) 423–425.
13	Ni–Al_2O_3 with SiO_2 ARC	R.F. Sputtering	Mo coated Ni coated Stainless steel	500˚C (1000 h) air	0.94	0.07	T.S. Sathiaraj, R. Thangaraj, A. Sharbaty, M. Bhatnagar, O.P. Agnihotri, Ni–Al2O3 selective cermet coatings for photothermal conversion up to 500°C, Thin Solid Films 190 (1990) 241–254.
14	Mo/HfOx/Mo/HfO2	Sputtering	Copper	500˚C (2h) in air 800˚C (2h) in vacuum	0.872	0.09	N. Selvakumar, Harish C. Barshilia, K.S. Rajam and A. Biswas, Solar Energy Materials & Solar Cells 94 (2010) 1412–1420.
15	TiAlN/SiCNH	magnetron sputtering and plasma-enhanced chemical vapor deposition	Inconel 625	500˚C (732 h) in air	~0.91	~0.31	Alex Carling-Plaza, Muhammad Asaad Keilany, Maxime Bichotte, Audrey Soum-Glaude, Laurent Thomas and Laurent Dubost, SolarPACES 2018, AIP Conf. Proc. 2126, 020001-1–020001-7; https://doi.org/10.1063/1.5117509
16	Al_xO_y/Pt/Al_xO_y	Electron beam evaporator	Copper	500˚C (2h) in air	0.937/0.930	0.10/0.11	Z.Y. Nuru, Renewable Energy 75 (2015) 590-597.
17	Ni/Ni–Al_2O_3	Vacuum evaporation	Quartz	500˚C (100 h) in air	0.96	0.22 at 150°C	H.G. Craighead, R.A. Buhrman, Optical properties of selectively absorbing Ni/Al2O3 composite films, Applied Physics Letters 31 (1977) 423–425.
18	Al_2O_3/Mo/Al_2O_3	RF Sputter	Mo coated Stainless steel	550˚C (14 h) in air	0.92-0.95	0.06-0.10@20oC	JOHN A. THORNTON, ALAN S. PENFOLD AND JAMES L. LAMB, Thin Solid Films, 72 (1980) 101-109.
19	Ni/Mo–TiC cermets	Spray and Laser cladding	Stainless steel	600˚C (1h) in air	0.80/0.807	0.055/0.06	Xuming Pang, Mater. Res. Express 4 (2017) 095503.
20	AlCrN/AlCrNO/AlCrO	Cathodic arc	304L Stainless steel	600˚C (2 h) in air	0.93/0.94	0.20/0.21	Dianqing Gong, et al., Solar Energy 180 (2019) 8–15.
21	cobalt oxide	spray pyrolyze aqueous	Stainless steel	600˚C (24 h) in air	0.80	0.15	C S UMA, L K MALHOTRA and K L CHOPRA, Bull. Mater. Sci., Vol. 8, No. 3, June 1986, pp. 385-389.
22	CuCoMnOx	Dip-coating	304L SS	600˚C (25 h) in air	0.90	0.10	Jie Min and Weiyang Guo, Advances in Materials Processing, 95-103. https://doi.org/10.1007/978-981-13-0107-0_9.
23	Pt/Al_2O_3	Co-evaporation	Pt coated Quartz	600˚C (300 h) in air	0.94	$0.19_{@150oC}$ $0.24_{@300oC}$ $0.33_{@500oC}$	H. G. CRAIGHEAD, R. BARTYNSKI, R. A. BUHRMAN, L. WOJCIK and A. J. SIEVERS, Solar Energy Materials 1 (1979) 105-124.
24	Ni/Al_2O_3	Co-evaporation	Ni coated Quartz	600˚C (300 h) in air	0.94	$0.22_{@150oC}$ $0.32_{@300oC}$ $0.45_{@500oC}$	H. G. CRAIGHEAD, R. BARTYNSKI, R. A. BUHRMAN, L. WOJCIK and A. J. SIEVERS, Solar Energy Materials 1 (1979) 105-124.
25	Cr/AlCrSiN/AlCrSiON/ AlCrO	cathodic arc ion plating	SS 304	600˚C (600 h) in air	0.950.924	0.14/0.16	Changwei Zou, Wei Xie, Lexi Shao, Solar Energy Materials & Solar Cells 153 (2016) 9–17.
26	TiN/$Al_yTi_{1-y}(OxN_{1-x})$	cathodic vacuum arc	Inconel HAYNES ® 230	600˚C (900 h) in air	0.91	0.14	R. Escobar-Galindo, et al., Solar Energy Materials and Solar Cells 185 (2018) 183–191.

27	Pt-Al_2O_3 cermet with Al2O3 ARC	RF-Sputtering	316 Stainless steel	600˚C (2000 h) in air	0.97	0.07@$_{20oC}$ 0.16@$_{500oC}$	John A. THORNTON and James L. LAMB, Solar Energy Materials 9 (1984) 415-431.
28	MoSi2- Si3N4/Al2O3	RF and DC Sputtering Al2O3 by ALD	Stainless steel	600˚C (2900 h) in air	~90.8/92.4	~48.0/46.3	Eva Cespedes, et al. , ACS Appl. Energy Mater. 2018, 1, 11, 6152-6160.

Table 3: Solar absorber coating stable in air above 600°C temperature.

S.No	Material	Deposition method	Substrate	Temperature (annealed in air)	Absorptance (α) (as depo. /after annealing)	Emittance (ε)	Figure of merit	Reference
1	TiN-TiC-Ni-Mo Cermet	Spray then laser cladding process	Stainless steel	650˚C (6 h) in air	0.801/0.808	0.024/0.019		Xuming Pang, Ye Shen, Jinyi Wei, Wenyu Yang, Applied Physics A (2019) 125:677.
2	TiC-Ni/Mo	Spray then laser cladding process.	316Ti stainless steel	650˚C (200 h) in air	0.86/0.85	0.04/0.047		Xuming Pang, Qian Wei, Jianxin Zhou and Huiyang Ma, Materials 2018, 11, 1037
3	RuO_2/SiO_2	dip coating	316L Stainless steel	650˚C (873 K) (1000 h) in air	0.94	0.28$_{@873K}$		Xavier Paquez, Guillaume amiard, Guillaume de Combarieu, Cédric Boissière, and David Grosso, Chemistry of Materials 27 (2015) 2711-2717
4-a	Co_3O_4 nanoneedle	Hydrothermal process	Haynes 230	650˚C (100 h) in air	0.99/0.948	No data		Elizabeth B. Rubin, Sunmi Shin, Yiming Chen, Renkun Chen, APL Materials 7 (**2019**) 131101(1-9)
4-b	Co_3O_4 nanoneedle/HfO_2	Hydrothermal process	Haynes 230	650˚C (100 h) in air	0.977/0.982	No data		Elizabeth B. Rubin, Sunmi Shin, Yiming Chen, Renkun Chen, APL Materials 7 (**2019**) 131101(1-9)
5	$MoSi_2$-$Si_3N_4/Si_3N_4/Al_2O_3$	Sputtering	Inconel 625	700oC (15 hrs) 600oC (475 hrs)	0.92	0.15$_{@25oC}$ 0.33$_{@600oC}$		Adrián Rodríguez-Palomo, Eva Céspedes, David Hernández-Pinilla, Carlos Prieto, Solar Energy Materials and Solar Cells 174 (2018) 50–55.
6	$MoSi_2/Al_2O_3$	Sputtering	Quartz	700 (300h) in air	0.92	0.14		J.H. Schon, G. Binder, E. Bucher, Performance and stability of some new ¨ high-temperature selective absorber systems based on metal/dielectric multilayers, Solar Energy Materials and Solar Cells 33 (1994) 403–416
7	Co_3O_4/SiO_2	Spray coating	Inconel 625	750 ◦C (1000 h) in air	--	--	88.2%	Jaeyun Moon, et al., Solar Energy Materials & Solar Cells 134 (2015) 417–424.
8	$CuFeMnO_4$(PT)/ $CuCr_2O_4$(DB)	spray-coated	Inconel 625	750 °C (500 h) in air	--	--	0.903/0.896	Tae Kyoung Kim et al., Solar Energy 132 (2016) 257–266.
9	$Si_{0.8}Ge_{0.2}$	Drop casting	Stainless steel	750˚C (1 h) in air	0.90-0.95	~0.30		Jaeyun Moon, et al., Nano Energy (2014) 8, 238–246.
10	Ni/NiSi core-shell structures embedded in the $SiO_{1.5}$	Spin coating	Stainless steel	750˚C (1000 h) in air	--	--	89.8$_{C=1000}$	Xiaoxin Wang, Xiaobai Yu, Sidan Fu, Eldred Lee, Katerina Kekalo, and Jifeng Liu, Journal of Applied Physics (2018) 123, 033104
11	Silicon-based Black Paint "CoteRill™ 750"	Spray Coating	Haynes 230	750˚C in air	0.972/0.962	--		Ridha Harzallah, Maiwenn Larnicol, Christophe Leclercq, Alexandre Herbein and Florent Campana, AIP Conference Proceedings 2126 (**2019**), 030026
12-a	$CuFe_{0.4}Mn_{1.4}O_{42}$-Bluesil Silicone cermet	Spray Coating	Inconel	750°C (1000 h)	0.967/0.976	0.55/0.73	0.9312$_{C=1000}$/ 0.9305$_{C=1000}$	Jifeng Liu, Assistant Professor; Dartmouth College; Final Technical Report
12-b	$MnFe_2O_4$-RSN Silicone	Spray coating	Inconel (textured by $HCl:H_2O_2$)	750°C (1000 h)	0.947/0.956	0.62/0.52	0.903$_{C=1000}$/0.915$_{C=1000}$	Jifeng Liu, Assistant Professor; Dartmouth College; Final Technical Report
13-a	Dense $Cu_{0.5}Cr_{1.1}Mn_{1.4}O_4$	Spray coated	Haynes 230	800˚C (2000 h) in air	0.960	0.801	0.908	Elizabeth B. Rubin, Yiming Chen, Renkun Chen, Solar Energy Materials & Solar Cells 195 (**2019**) 81–88.
13-b	Dense $CuCr_2O_4$	Spray coated	Haynes 230	800˚C (2000 h) in air	0.973	0.924	0.914	Elizabeth B. Rubin, Yiming Chen, Renkun Chen, Solar Energy Materials & Solar Cells 195 (**2019**) 81–88.
13-c	Porous $CuFeMnO_4$/dense $CuCr_2O_4$	Spray coated	Haynes 230	800˚C (2000 h) in air	0.953	0.899	0.895	Elizabeth B. Rubin, Yiming Chen, Renkun Chen, Solar Energy Materials & Solar Cells 195 (**2019**) 81–88.
13-d	Pyromark 2500	Spray coated	Haynes 230	800˚C (2000 h) in air	0.964	0.920	0.905	Elizabeth B. Rubin, Yiming Chen, Renkun Chen, Solar Energy Materials & Solar Cells 195 (**2019**) 81–88.

13-e	Porous $Cu_{0.5}Cr_{1.1}Mn_{1.4}O_4$	Spray coated	Haynes 230	800˚C (2000 h) in air	0.971	0.886	0.914	Elizabeth B. Rubin, Yiming Chen, Renkun Chen, Solar Energy Materials & Solar Cells 195 (**2019**) 81–88.
4-c	$CuCo_2O_4$ nanoneedle	Hydrothermal process	Haynes 230	800˚C (100 h) in air	0.993/0.967	No data		Elizabeth B. Rubin, Sunmi Shin, Yiming Chen, Renkun Chen, APL Materials 7 (**2019**) 131101(1-9)
4-d	$CuCo_2O_4$ nanoneedle/SiO_2	Hydrothermal process	Haynes 230	800˚C (100 h) in air	0.995/0.993	No data		Elizabeth B. Rubin, Sunmi Shin, Yiming Chen, Renkun Chen, APL Materials 7 (**2019**) 131101(1-9)
14	MoS_2–SiO_2	Spin coating	Stainless steel	850˚C (100h) in air	0.950/0.946	0.937/0.920	86C=1000	Yijie Liu et al., Solar Energy Materials and Solar Cells 200 (**2019**) 109946 (1-6)
15	black chrome/ITO/SiO2	Electroplating (black chrome), Sputtering (ITO, SiO2)	Stainless steel	900˚C (60h) in air	0.95/0.90	0.2/0.4		Hao Wang, Iwan Haechler, Sumanjeet Kaur, Justin Freedman, Ravi Prasher, Solar Energy 174 (**2018**) 305–311

A.1.2. Figure of Merit (FOM)—Absorber Efficiency (η)

Considering the different operating temperatures and solar concentration values in CSP plant operation, it is desirable to compare the coatings on a common basis for application to the four types of CSP plants. Linear Fresnel reflectors (LFRs) and parabolic collectors (PTCs) operate in a temperature range 300 °C to 400 °C with concentration ratios of 30 and 80, respectively. However, high-temperature power plants using central receiver/power tower and parabolic dishes operate in 400 °C to 750 °C with a concentration ratio of 1000 and 1500, respectively. For PTCs and LFRs operating at relatively low temperatures, the heat loss from the receivers critically affects the thermal efficiency of the receiver. Nevertheless, the next-generation solar tower and parabolic dishes are aimed to work at a very high temperature of ~750 °C and a concentration of ~1000 suns; for which more than the radiative heat loss, the solar absorptance and high-temperature stability in an open-air environment are the major factors of an absorber to be optimized.

Since the optical data of solar absorber coatings in the various sources in the literature are all based on different conditions, they are compared on a common basis by evaluating a figure of merit (FOM) using the reported absorptance and emittance values. The FOM of different types of solar absorber may be evaluated using the following expression for the solar absorber efficiency:

$$\eta = \frac{\alpha Q - \varepsilon \sigma T^4}{Q} \quad (1)$$

where α is the solar absorptance, Q is the irradiance on the receiver, ε is the thermal emittance, σ is the Stefan-Boltzmann constant and T is the absolute surface temperature in units of Kelvin. In this study, we calculated the efficiency of solar absorbers for Gen3 power tower systems, by assuming the black body temperature T = 750°C and the concentration ratio C to be 1000 (1000 sun), which are the target temperature and concentration ratio, respectively, for Gen3 CSP systems as defined in the SOPO.

Table 4 summarizes the absorber efficiency values and the maximum temperature stability for the various coatings grouped by the four different types discussed earlier in this section. Note that based on the maximum temperature stability, not all coatings are viable at the temperature of 750°C targeted for Gen3 systems. The coatings that are suitable for the Gen3 temperatures are highlighted in green in the Table 4. From this literature survey, based on purely thermal efficiency consideration, we can see that nanostructured spinel oxides of $CuFeMnO_4$, $CuCr_2O_4$, $MnFe_2O_4$, Co_3O_4, and $CuCo_2O_4$, etc. and metal/metal silicide like $Ni/NiSi_2$, $Ni/TiSi_2$ could be candidate solar absorber coatings for the high temperature (>750°C) Gen 3 CSP applications.

Table 4: Absorber efficiency and temperature stability in air of different types of solar absorber coatings.

	Efficiency at ~1000 sun	Maximum Temperature Stability (°C)
Dielectric/Metal/Dielectric		
MgO/Zr/MgO	90.25	250
$CrO_y/Cr/Cr_2O_3$	89.42	300
$Al_2O_3/Mo/Al_2O_3$	93.56	300
$HfO_x/Mo/HfO_2$	91.26	400
$Al_xO_y–Al–Al_xO_y$	95.76	400
$HfO_x/Mo/HfO_2$	89.14	500
$HfO_x/Mo/HfO_2$	90.44	500
$Al_2O_3/Mo/Al_2O_3$	91.62	550
$Al_xO_y/Pt/Al_xO_y$	93.07	500
$Al_xO_y/Pt/Al_xO_y$	95.16	500
$Al_xO_y/Pt/Al_xO_y$	93.24	700
Graded Multilayer		
$CrN(H)/CrN(L)/CrON/Al_2O_3$	92.13	400
$W/WAlN/WAlON/Al_2O_3$	89.06	400
$HfMoN(H)/HfMoN(L)/HfON/Al_2O_3$	93.19	475
TiAlN/SiCNH	89.07	500
$TiN/Al_yTi_{1-y}(O_xN_{1-x})$	90.13	600
AlCrN/AlCrNO/AlCrO	91.75	600
AlCrSiN/AlCrSiON/AlCrO	94.13	600
$MoSi_2\text{-}Si_3N_4/Al_2O_3$	87.81	600
$MoSi_2\text{-}Si_3N_4/Si_3N_4/Al_2O_3$	91.06	700
Black chrome/ITO/SiO_2	93.75	900
Cermet		
Au-MgO	89.37	400
Al/AlN	92.75	400
Ni/MgF_2	95.19	450
$Ni\text{-}Al_2O_3/Al_2O_3$	93.37	500
$Ni\text{-}Al_2O_3/SiO_2$	93.56	500
$Ni/Ni\text{-}Al_2O_3$	94.63	500
Ni/Al_2O_3	92.63	600
Pt/Al_2O_3	92.81	600
TiN-TiC-Ni-Mo	79.95	650
$Ni/NiSi\text{-}SiO_2$	89.8	750

MoSi2-SiO2	89.17	850
Oxide coating		
Co_3O_4-Fe_2O_3	92.75	400
Co_3O_4	97	400
Mn-Cu-Fe oxide	90.31	500
CrAlO	91.37	500
Co_2O_3	79.06	600
CuCoMnOx	89.37	600
Pyromark 2500	90.54	650
RuO_2/SiO_2	92.26	650
Co_3O_4 nanoneedle/HfO_2	94.59	650
Co_3O_4 nano needle	95.89	650
Co_3O_4/SiO_2	88.2	750
$MnFe_2O_4$.RSN	90.84	750
$Cu_{0.15}Co_{0.284}O$ with texturing	90.26	750
$Cu_{1.5}Mn_{1.5}O_4$ with texturing	90.90	750
CoteRill™ 750	92.22	750
$CuFe_{0.4}Mn_{1.4}O_4$	93.28	750
Porous $CuFeMnO_4$/Dense $CuCr_2O_4$	89.73	800
Dense $Cu_{0.5}Cr_{1.1}Mn_{1.4}O_4$	91.02	800
Dense $CuCr_2O_4$	91.55	800
Porous $Cu_{0.5}Cr_{1.1}Mn_{1.4}O_4$	91.59	800
$CuCo_2O_4$ nanoneedle	96.19	800
$CuCo_2O_4$ nano needle/SiO_2	96.39	800

A.2. M(ST-1.1) Experimental Design Matrix

We designed an experimental matrix that contains the list of coating materials, substrates, substrate finishes, deposition conditions. The coating materials are selected based on the literature review summarized in Section A.1. Textured absorber coatings were fabricated on different high-temperature stable substrates, Inconel 625, Inconel 718, Hynes 230, Inconel 800H, and Stainless steel 316 (SS-316). The optical properties and uniformity of electrodeposited surfaces strongly depend on the electrodeposition conditions and substrate preparation methods. Therefore, the effects of applied overpotential, deposition duration, and electrode distance on the optical properties of different electrodeposited solar selective coatings were comprehensively studied. To study the effect of various substrate finishes on optical properties, we coated some absorber materials on as-received, polished and etched substrates.

A.2.1. ST-1.2 Electrodeposition Procedure

An AUTOLAB PGSTAT128N potentiostat supplied by ECO chemie, Utrecht, The Netherlands, was used to perform the electrodeposition experiments. The electrodeposition process employed the traditional three-electrode system, with 15 cm^2 platinum mesh as a counter electrode (C.E.), Ag/AgCl as a reference electrode (R.E.), and metal substrate sheet with an exposed area of 12.25 cm^2 as the

working electrode (W.E.). All the electrodes were rigorously cleaned in an ultrasound cleaner with deionized water, acetone, and 2-propanol to remove any dirt and grease from their surfaces and dried in air. The counter electrode was kept equidistant, d, from the R.E. and C.E. Figure 1 shows a schematic diagram of the experimental setup. All the metal oxides were deposited from their corresponding 0.05M metal nitrate/s aqueous solution containing 0.1M KNO_3.

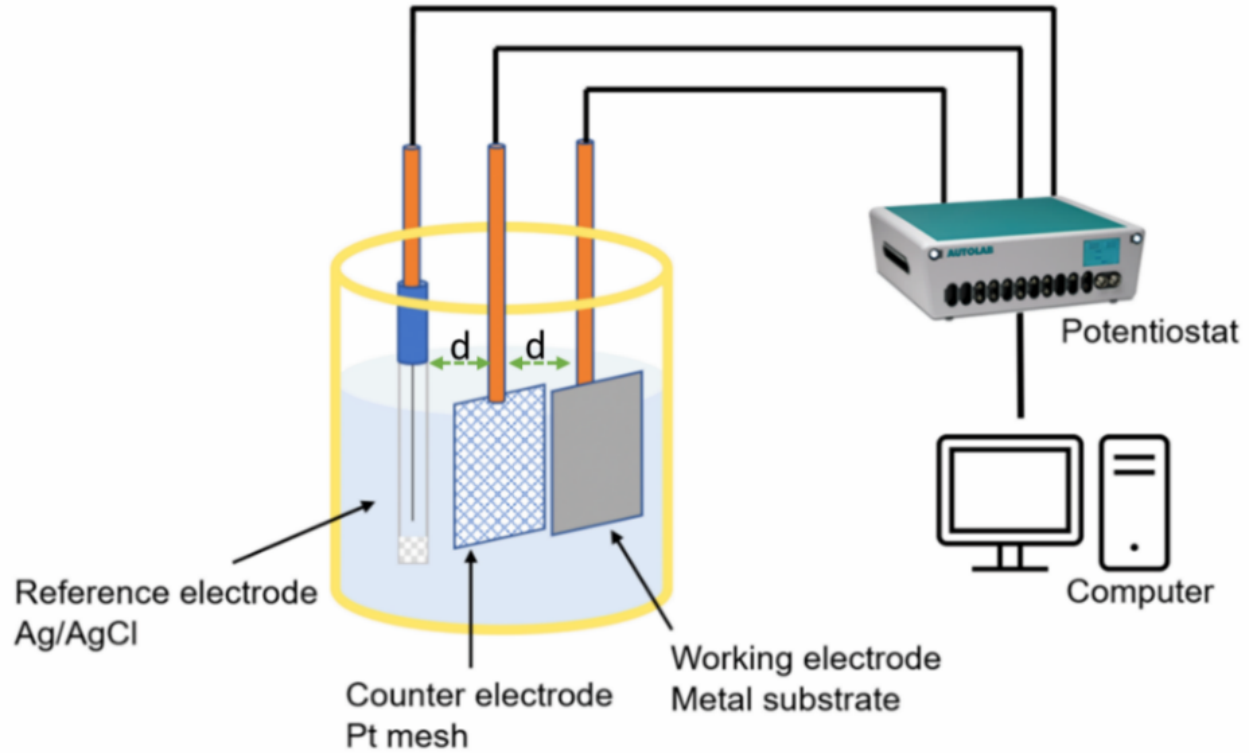

Figure 1: Schematic representation of the electrodeposition cell and arrangement of working, counter, and reference electrodes during the electrodeposition process. "d" is the distance between electrodes.

A.2.2. Optical Properties Characterization

Spectral total absorptance (1-reflectance) of the absorber coatings was recorded in the 250 to 2500 nm wavelength range using a Cary 5000 UV-Vis-NIR spectrophotometer equipped with an integrating sphere. A PTFE reflectance standard was used to calibrate the instrument before the actual measurement. Additionally, the spectral total absorptance (1-reflectance) of the absorber coatings from 2500 to 15000 nm was measured using a Varian 670 FTIR spectrophotometer, which was equipped with a Pike® mid-IR integrated sphere. Emittance values were calculated from the FTIR spectra using a dedicated software program at different temperatures. Also, the average solar absorptance of each coating was measured as per ASTM G173 standard using a solar spectrum reflectometer (Model SSR) of Devices and Services illuminated by a tungsten-halogen lamp and calibrated using a standard sample. The radiation reflected by the sample was measured at an angle of 37° from the normal, with four filtered detectors (UV, blue, red, and infrared). Solar spectrum absorptance measurement was achieved by adding the four outputs in the appropriate proportions. The infrared emittance of each coating was measured corresponding to a temperature of 100 °C using a Devices and Services (D&S) emissometer (Model AE) calibrated using standard samples and with a measurement repeatability of 0.01 units. The emissometer was heated to 100 °C so that the sample to be measured need not be heated. At 100 °C, the spectral range of the thermal radiation emitted from the surface is in the range of 3–30 μm.

A.2.3. Optimization of Deposition Parameters

The effects of electrodeposition conditions—deposition voltage, distance between electrodes, and deposition duration—on the optical properties were comprehensively studied with a view to determining the optimum combination of parameters. ***The highest efficiency was achieved for samples prepared while keeping the electrodes 2 cm apart.***

A.2.4. Effect of Substrate Materials on Optical Properties

For next-generation CSP applications, selecting the substrate material is critical because substrate breakdown at high temperatures is a significant issue that must be addressed for success. Therefore, the absorber coating and coating methods should be applicable to any substrate material suitable for practical applications. To study the effect of substrate materials on optical properties, we deposited different absorber coatings on various substrates: Inconel 625, Haynes 230, Inconel 718, Inconel 800H, and SS-316. ***From this study, we observed that it is possible to fabricate high-efficiency absorber coatings on any potential high-temperature stable substrate using electrodeposition.***

A.2.5. Effect of Substrate Finish on Optical Properties

We further studied the effect of substrate finishing on the optical properties of black absorber oxides deposited on as-received, polished, and etched Inconel 625 substrates at different voltages. We selected Inconel 625 substrates for this study. The Inconel 625 substrates were etched using a solution of H_2O_2, HCl, and HNO_3 in a ratio of 18:12:6 for 40 minutes. The polished substrates were prepared by mechanically grinding the substrates using SiC paper with grit sizes ranging from 120 to 1200. After grinding, the substrates were polished with a 0.2µm grit size diamond suspension. ***The efficiency of the coatings was found to be the same for different substrate finishes. Therefore, in all further studies, we used as-received Inconel 625 substrates without any surface treatment except for cleaning with soap solution, followed by ultrasound cleaning in DI water, acetone, and 2-propanol.***

A.3. ST-1.2, ST-2.1 Fabrication of Fractal Textured Surfaces on a Range of Materials

We studied the possibility of texturing different black oxide coatings using the electrodeposition method for CSP application. Many single, double, and triple metal oxides were prepared by electrodeposition and their optical properties were evaluated. The efficiency of the coatings was calculated from the absorptance and emittance study, and coating materials that show an efficiency higher than 93%, as required by the metrics of the current project, were selected for further studies. Based on the experimental matrix, we deposited single layers and multilayers of different single metal oxides, double metal oxides, triple metal oxides. ***This study showed that single, double, and triple metal oxides can be electrodeposited on Inconel 625 substrates, and the texturing can be adjusted by varying the electrodeposition voltage and deposition times. Double metal oxides show the highest efficiency, greater than 93%. When the coatings are deposited in multiple layers, the efficiency increases to greater than 95%.***

A.3.1. X-ray Diffraction (XRD) Studies

XRD spectra were taken to study the structural evaluation of black absorber coatings via electrodeposition at different overpotentials and subsequently annealed for two hours in air. A Bruker D8 Advance X-ray spectrophotometer was used to record the crystallographic data of the coatings. The XRD spectra showed that the electrodeposition voltage played a critical role in forming the spinel structure during electrodeposition.

A.3.2. Surface Morphology of black absorbers

Surface morphology and cross-sectional images of black absorbers were taken using scanning electron microscopy assisted with a focused ion beam. It is evident that the absorber coatings exhibit multi-scale features spanning from a few micrometers to the nanometer scale on the substrate surface. Cross-sectional images of a black absorber coating at different magnification levels, shown in Figure 2 (a) and (b), reveal a multi-textured surface with flower-like structures at the bottom and web-like structures at the top, with a total thickness of approximately 3 μm. The microporous top layer and nanostructured bottom layer are suitable for trapping the visible region of the solar spectrum. These micro gaps and nanostructured bottom layers also help trap visible light and enhance the overall efficiency of the surfaces.

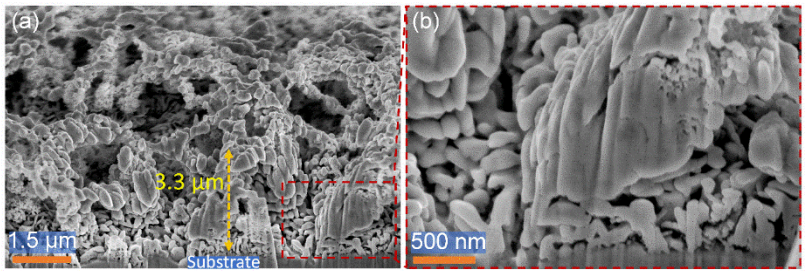

Figure 2: Cross-section FIB-FESEM images of a black absorber coating at different magnifications.

A.3.3. Energy-dispersive X-ray Spectroscopy (EDS)

Energy dispersive X-ray spectroscopy (EDS) was used to confirm the presence of elements in the coating. Quantifying the elements from the EDS spectrum of each coating proved challenging due to the highly textured nature of the coating. There was some variation in the atomic percentage of the coating elements from one location to another. Nevertheless, in all locations, we identified elements corresponding to the coating material. Therefore, the EDS analysis confirms that the coatings consist of the corresponding elements in the coating composition.

A.4. ST-1.3 M(ST-1.3) Power Spectra and Fractal Dimensions

The fractal structure of the electrodeposited surface was determined from the power spectrum obtained from FESEM images using Gwyddion software to determine the scale-independent multiscale fractal nature of the absorber coatings. Using the obtained power spectra for the individual surfaces, their corresponding fractal parameters were calculated.

The fractal description used here is based on the Weierstrass-Mandelbrot (W-M) function and size distribution, wherein a surface profile is expressed as a summation of an infinite series of sinusoidal functions with different amplitudes and frequencies, which correspond to the height and length of multiscale asperity features, respectively. The Weierstrass-Mandelbrot (W-M) function has been extensively used in the analytical representation of multiscale featured surfaces in different applications [1–3]. For these non-differentiable surfaces, as progressively increasing roughness features are observed at progressively decreasing length scales; however, these surfaces can still be considered continuous as length scales are above atomic levels. The W-M function is a self-similar, non-differentiable, and continuous function that captures all the inherent characteristics of fractal surfaces. For electrodeposited multiscale surfaces, the surface profile, $z(x)$, can be expressed as:

$$z(x) = G^{D-1} \sum_{n=n_1}^{\infty} \frac{\cos(2\pi\, \gamma^n x)}{\gamma^{(2-D)n}} \tag{2}$$

where D is the fractal dimension, G is a mathematical scaling constant, γ^n is a frequency mode corresponding to the horizontal dimension, L, of roughness feature as $\gamma^n = \frac{1}{L}$, and γ^{n_1} corresponds

to the cut-off frequency, which relates to the maximum asperity length scale of the surface. Following [3,4], $\gamma = 1.5$ to represent the random phases in a roughness profile.

Power spectra of fractal objects are generally employed to describe their fractal properties for naturally occurring fractals and have been considered to describe and study the coated multiscale surfaces. Power spectrum of a surface is a mathematical tool that decomposes the surface into contributions from different spatial frequencies. It provides a representation of the amplitude of a surface's roughness as a function of the spatial frequency of the roughness. Spatial frequency is the inverse of the wavelength of the roughness features. Power spectrum of a surface is estimated as a square of surface profile's Fourier spectrum. The power spectrum of the W-M function, equation (2), exhibits a power law dependence on the spatial frequency, ω, given by:

$$S(\omega) = \frac{G^{2(D-1)}}{2\ln(\gamma)} \frac{1}{\omega^{(5-2D)}} \tag{3}$$

The fractal parameters of an actual surface profile are obtained by comparing its power spectrum to the power spectrum of the W-M function (equation 2).

Figure 3 show an SEM image of an electrodeposited absorber coating and the corresponding spectrum. In Figure 3(b), the abscissa represents the spatial frequency, which is inverse of asperity feature length scale and ordinate represents the power at specific spatial frequency, which is obtained from a fast Fourier transform (FFT) of the three-dimensional surface profile using the Gwyddion software. Note that the power spectrum is presented on a log-log scale. It can be seen from Figure 3 (b) that the power law variation holds within a frequency range that is characteristic for each surface, as also previously reported by Majumdar and Bhushan [3] and Yang and Pitchumani [4]. The high frequency limit of the range corresponds to the length of the smallest asperity on the surface under study and the low-frequency limit corresponds to the largest repeating unit or the largest asperity length scale present on the surface. Further, it follows from equation 2 that the slope of the linear variation of data in the range of frequencies equals $(2D - 5)$, and the intercept on the ordinate relates to the scaling constant G. The fractal dimension for the surface shown in Figure 3(a) was observed to be 1.81 due to the highly textured morphology of the deposited coatings.

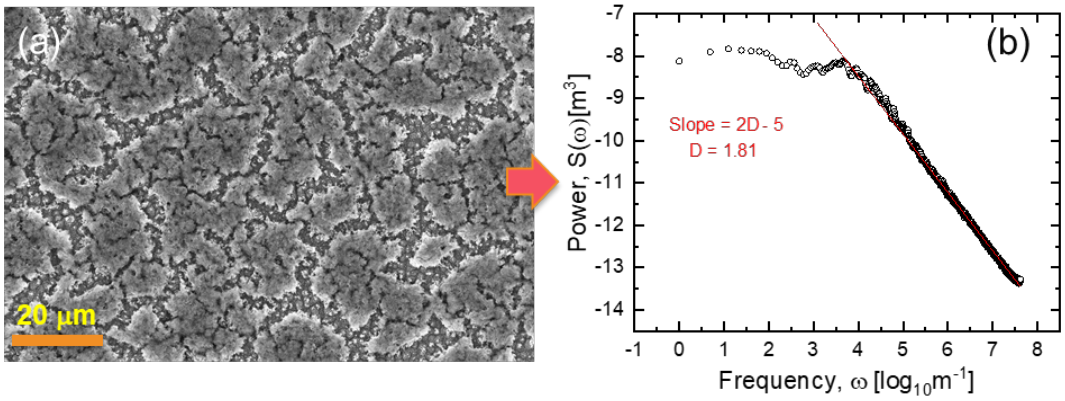

Figure 3: (a) FESEM image and (b) corresponding fast Fourier transform-based power spectrum of absorber coating.

We prepared ten replicates of different absorber coatings on Inconel 625 substrates to assess the consistency of textured property and fractal existence of the electrodeposited surfaces, and measured their fractal dimension from FESEM images. We found that all the samples exhibit fractal dimensions greater than 1.5. Moreover, due to the highly multiscale structure of the electrodeposited absorber coatings, the measured fractal dimensions were in the range 1.77–1.89 for all the coatings. This study shows that electrodeposition process yields samples consistent in morphology and fractal dimensions.

As required to complete the **M(ST-1.3)** milestone, we performed the one-tailed Student t-test at 95% confidence level to show the samples are more significant than 1.5 fractal dimensions.

B. Optical and Mechanical Characterization of Absorber Surfaces—M(ST-2.1), G/NG-1

B.1. Simulation of Optical Properties of Fractal Surfaces

Simulation studies were also conducted to gain further fundamental understanding on the interaction of fractal texturing with solar radiation and its effects on the optical properties [5,6]. The goal of the studies was to understand how interaction of solar radiation with simulated fractal textured surfaces affects the absorptance. To this end, two types of fractal surfaces were generated, one based on the Koch curve and the other based on the W-M function. In each case, the texturing was systematically increased in its multiscale features to see how the number of generations in the Koch curve or the fractal parameters of the W-M function affected the absorptance of the surface.

B.1.1. Optical Modeling of Rough Surface

Figure 4 schematically represents the interaction of solar radiation with a plane surface (Figure 4(a)) and two different types of simulated rough surfaces. Figure 4(b) and Figure 4(c) represent fractal surfaces comprising the Koch curve and W-M function, respectively, at their respective different roughness parameters. Since an optical wave is a type of electromagnetic wave that propagates as per Maxwell's equations, electromagnetic theory is used to investigate the effect of surface morphology and surface roughness on material absorptivity. Maxwell's equations can be expressed as:

$$\nabla \times (\nabla \times E) - k_0^2 (n - ik)^2 E = 0 \tag{4}$$

where E represents the electric field, k_0 is the wavenumber of free space, n and k are the real and imaginary parts of the refractive index, respectively. In two-dimensions, the electric field varies with the out-of-plane wave number k_z as follows, where z is the unit vector in the out-of-plane z-direction:

$$E(x, y, z) = \tilde{E}(x, y)^2 e^{-ik_z z} = 0 \tag{5}$$

Figure 5 presents the computational domain for the model of a rough surface. Light is launched from an interior plane (dashed line) toward the material interface. Light reflected back toward the source plane passes through it and is absorbed by a perfectly matched layer (PML). One additional boundary is introduced to monitor the total reflectance in between PML and source plane. At this boundary, the power flux is integrated with the upward direction, normalized by the incident power, which gives the total reflectance.

To accurately determine the integral of the power flux at this boundary, a boundary layer mesh composed of a single layer of elements much smaller than the wavelength is introduced. The PML absorbs both the propagating and evanescent components of the field, but only the propagating component is required to be absorbed. Therefore, the PMLs should far enough away from the material interfaces. To satisfy this condition, the PML should at least half a wavelength away from the material interfaces. The results of the simulations are discussed in terms of the spectral reflectance, which may be regarded as the ones complement of the spectral absorptance: $R(\lambda) = 1 - \alpha(\lambda)$.

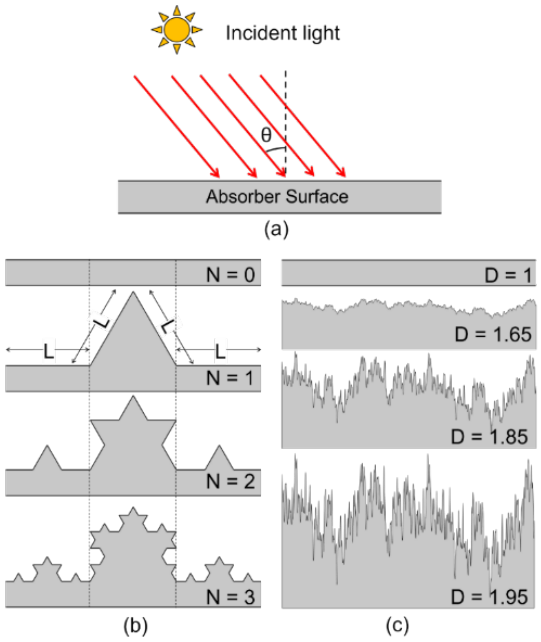

Figure 4: Description of (a) plane surface, and rough surfaces formed as (b) Koch curves at multiple generations and (c) Weierstrass–Mandelbrot (W–M) function.

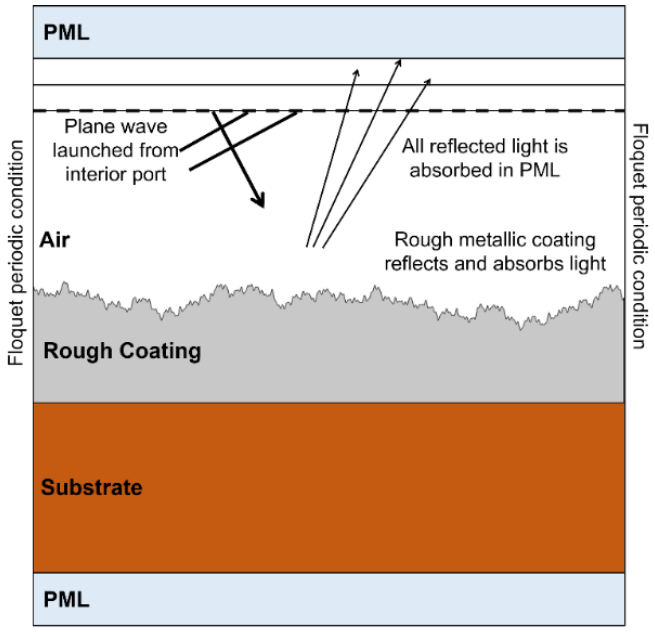

Figure 5: Computational model of the rough surface.

B.1.2. Effect of Roughness Parameters on Absorptance

The spectral variation of the reflectance at different light incident angles ($\theta = 0^o, 30^o, 45^o, 60^o, 75^o$) and different roughness parameters for the Koch curve are presented in Figure 6. The parametric study is conducted for three different generations, N (1, 3, and 5) and three different facet length values L (1 µm, 2.5 µm, and 5 µm). The effect of N on the spectral variation reflectance at different L can be seen in Figure 6, moving from left to right, and the effect of L can be observed moving from top to bottom. Figure 6(a-c) represents the reflectance at 3 different N and constant L = 1 µm. From Figure 6(a-c), it can be noticed that the reflectance is decreasing with increasing N; with increasing N, the number of roughness asperities increases which decreases the specular reflection from the surface, consequently improving absorptance. A similar trend is observed for L = 2.5 µm (Figure 6(d-f)) and L = 5 µm (Figure 6(g-i)). Further, it can be seen that for constant N, the reflectance decreases with increasing L, as the surface area is higher for larger L, which facilitates greater light trapping.

Figure 7 represents the spectral variation of the reflectance at different light incident angles ($\theta = 0^o, 30^o, 45^o, 60^o, 75^o$) for different fractal dimension D and scaling factor G of W-M function. The effect of increasing fractal dimension D and scaling factor G on the spectral variation of reflectance can be observed by moving from left to right and top to bottom, respectively in Figure 7. With an increase in the D value, the surface roughness increases which, in turn, increases the light trapping in between the asperities; therefore, the reflectance (absorptance) over the rough surface decreases (increases). Further, the reflectance (absorptance) also decreases (increases) with an increase in the scaling factor G because of the accompanying increase in the asperity height.

The simulation results demonstrate that fractal texturing has a beneficial effect on the optical properties of absorber coatings for CSP applications, supporting the experimental findings.

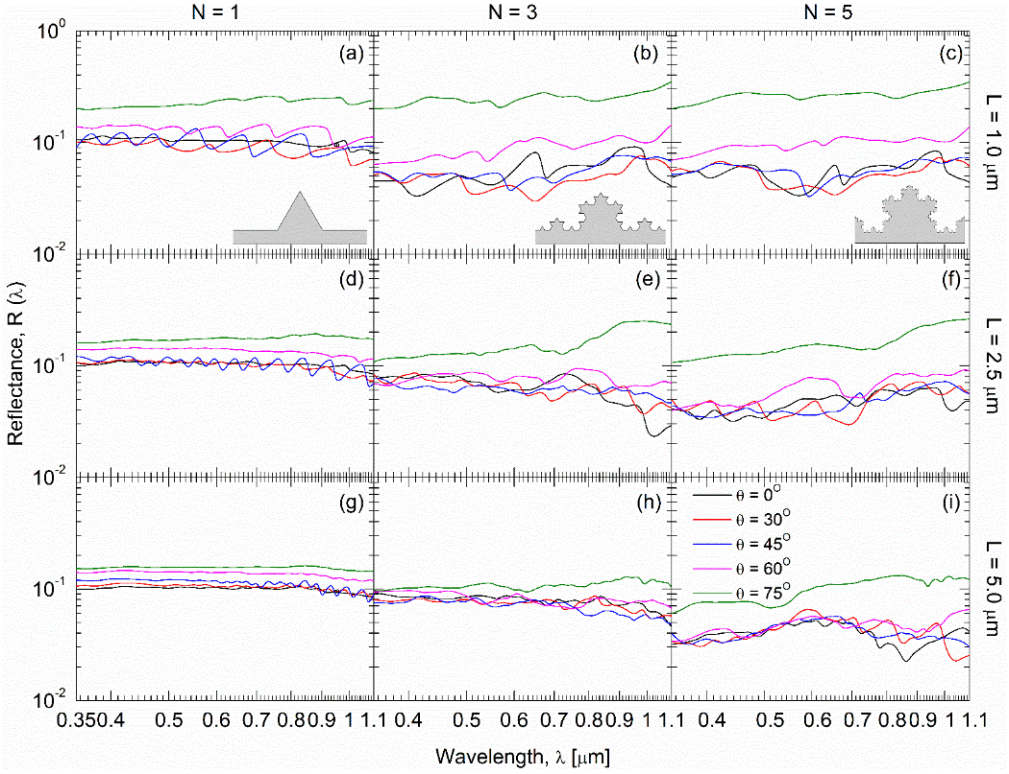

Figure 6: Spectral variation of reflectance at different incident angles; (a-c) at N = 1, 3, 5 and L = 1.0 μm, (d-f) at N = 1, 3, 5 and L = 2.5 μm, (g-i) at N= 1, 3, 5 and L = 5.0 μm.

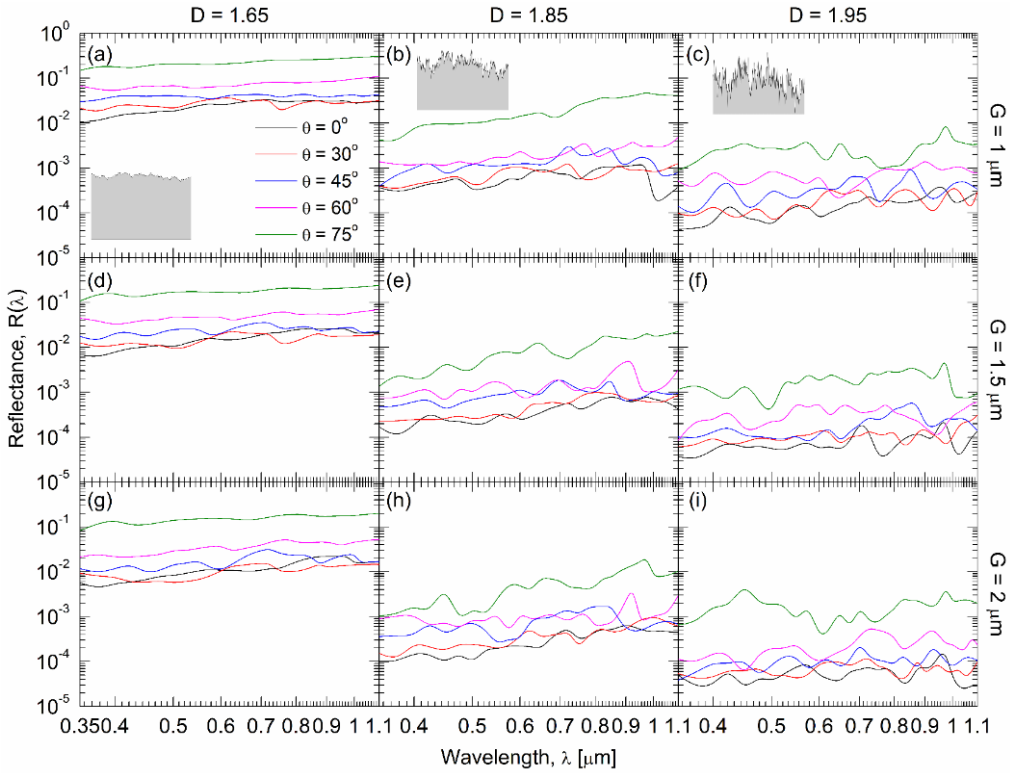

Figure 7: Spectral variation of reflectance at different incident angles for (a-c) D = 1.65, 1.85, 1.95 and G = 1.0 μm, (d-f) D = 1.65, 1.85, 1.95 and G = 1.5 μm, (g-i) D = 1.65, 1.85, 1.95 and G =2 μm.

B.2. Demonstration of Absorber Efficiency > 93%

Ten replicates of each absorber coating were prepared on Inconel 625 substrates at their respective optimum fabrication parameters. To prove their statistical significance, a one-tailed t-test was conducted on the performance of the 10 replicates. The findings showed that all the optimized black absorber coatings exhibited absorber efficiency greater than 93% at the 95% confidence level.
However, based on this study we found that novel multilayer cobalt-nickel oxide coating (here after it is also referred as m-CNO) are the best suitable absorber coating with absorptance >0.98 and initial efficiency >95%. Therefore, we selected multilayer cobalt-nickel oxide fabricated using the optimized deposition conditions for the isothermal and thermal testing as well as the cyclic thermal testing.

B.3. ASTM Mechanical Durability Tests

Adhesion, water immersion, and sand abrasion tests were conducted to assess the mechanical durability and the optical performance integrity of coatings deposited on Inconel substrates. The adhesion test was performed by securely affixing the sample to a benchtop with adhesive tape applied to the sides, followed by the application of the 3M Scotch® 250 tape to the surface. A one-pound roller was then rolled over the tape twice to ensure that the Scotch tape was well-adhered to the surface. The tape was then peeled off. Following the test, the tape was examined to investigate any coating removal. Further, absorptance and emittance of the coatings were measured both before and after the adhesion test.

A water immersion test was carried out following the ASTM D870 standard, wherein the sample was immersed in running water for one hour. Absorptance and emittance were measured 5 minutes after the samples were removed from the water and wiped dry, and then measurements were repeated 24 hours after the test. The post-test samples were also visually examined for any blistering defects or other signs of coating damage.

Mechanical durability of the coatings was further evaluated by performing a falling sand abrasion test based on the ASTM D968 standard. SiC grains (100−250 μm in diameter) were impinged on the samples inclined at an angle of 45°, from a height of 90 cm at a rate of 10 g/sec. In the present study, the durability of the coatings is defined as the ratio of absorber efficiency after and before the sand abrasion test. After every 10g of grain flow, we measured the absorptance and emittance of the coatings and calculated the efficiency.

All the absorber coatings showed excellent mechanical durability on the Inconel substrates.

C. Thermal Endurance Characterization—M(ST-3.2), M(ST-3.3), M(ST-3.4)

This section details the thermal endurance testing of the coatings identified so far with the goal of developing suitable candidates for the next-gen CSP receiver with efficiency greater than 93%. Isothermal testing was conducted at 750 °C for 100 hours and 750 hours to characterize the long-term durability of the electrodeposited absorber coatings. The optical properties of black absorbers were recorded before isothermal heating and after 12 hours and 100 hours of annealing durations.

Furthermore, day-night thermal cyclic tests were conducted to simulate the coating behavior in the real-world application. The sample was heated to 750 °C and held for 12 hours at that temperature; after 12 hours, the samples were allowed to cool for the next twelve hours. At the end of each heating/cooling cycle, absorptance and emittance were measured, from which absorber efficiency was calculated. Mechanical durability tests were also conducted after 50 thermal cycles to demonstrate the robustness of the coatings.

C.1. Isothermal Endurance Test of m-CNO Coatings at 750 °C for 100 hours in air — ST-3.1, ST-3.2, M(ST-3.2)

Ten replicas of optimized m-CNO coatings were subjected to isothermal heating at 750 °C in air for 100 hours. The initial absorptance of m-CNO dropped slightly after 12 hours of heating at 750 °C but the coating absorptance remained relatively constant between 12 and 100 hours of heating. Furthermore, the emittance decreased after a 12-hour heat treatment, but upon extending the heat treatment to 100 hours, it slightly increased, though it remained lower than the initial emittance value. Due to the decrease in absorptance and emittance of multilayer coatings, efficiency also decreased from 95.06% to 93.63% after 12 hours of heating. However, at the end of the 100 hours of isothermal heat treatment, m-CNO coatings showed average efficiency of 93.01%.

The absorber efficiency ratio of m-CNO after the isothermal test to before the isothermal test was calculated and is presented in Figure 8. The figure shows that m-CNO has an average efficiency ratio of more than the target of 0.98, with all values above 0.98, which is in the acceptable range.

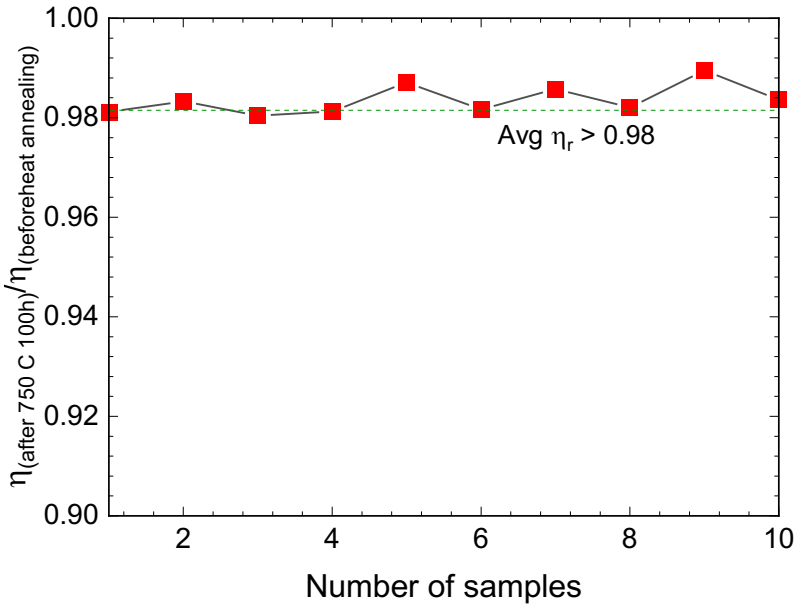

Figure 8: Efficiency ratio of m-CNO coatings after the isothermal test at 750 °C for 100 hours to before annealing.

To prove its statistical significance, one-tailed Student t-test findings of absorber efficiency and absorber efficiency ratio of 10 replicates of m-CNO coatings**.** According to the t-test data the average efficiency ratio is 0.984, which is greater than the postulated value of 0.98.

Mechanical endurance tests also showed that m-CNO coatings are mechanically robust after 100 hours of annealing at 750 °C. The absorptance was stable after the adhesion test, but the emittance decreased marginally after the adhesion test. Therefore, the efficiency of m-CNO coatings was improved slightly after the adhesion test, resulting in an absorber efficiency ratio of 1. Optical properties were found to be stable after a high-temperature quenching test, with an absorption efficiency ratio of 1 throughout the replicates, signifying no deterioration of the coating integrity or properties when subject to thermal shock. Optical properties and efficiency were also found to be stable after the water immersion test. The efficiency ratio was uniformly 1 signifying no deterioration. Mechanical durability of the m-CNO coatings after 750 °C, 100-hour thermal exposure was evaluated by performing a falling sand abrasion test based on the ASTM D968 standard. The durability of the coatings is defined as the ratio of absorber efficiency after to before the sand abrasion test. the

efficiency ratio decreases with abrasion grain mass, as expected. This aggressive abrasion test showed that the m-CNO coatings withstood a high SiC mass; initially, the absorber efficiency decreased abruptly with the abrasion grain mass but after 200g of SiC grain flow coatings showed a low degradation rate. Even after 400g of grain fell on the m-CNO coatings, the ratio of absorber efficiency after and before the sand abrasion test remained above 0.95 for all the coatings, which shows the superior mechanical property of m-CNO coatings after 750 °C, 100-hour isothermal exposure.

C.2. Isothermal Endurance Test of m-CNO Coatings at 750 °C for 750 hours in air M(ST-3.3)

Six replicas of m-CNO coatings were prepared and heated at 750°C for 750 hours in an air furnace. The coatings had an initial efficiency > 93% and the optical properties of the six replicas were measured at intervals of 12, 36, 50, 100, 500, and 750 hours. While heating m-CNO coating, emittance decreased at the initial stage of heat treatment. However, further increase in the heating duration led to an increase in emittance however, still which is lower than the initial emittance of the as-prepared m-CNO coatings. The efficiency of m-CNO decreased from 95.1% to 93% after 100 hours of heat treatment, and the efficiency after 750 hours of isothermal testing was 92%. The efficiency ratio of m-CNO coatings after 750 hours of isothermal test at 750 °C to the efficiency before the test is given in Figure 9. ***The average ratio of the absorber efficiency before and after the isothermal annealing at 750 °C for 750 hours of the six m-CNO replicates was 0.97***. This value exceeds our postulated absorber efficiency ratio, 0.95, for the project demonstrating the superior thermal stability of the coatings over extended isothermal exposure. Therefore, we can confidently state that m-CNO coating can be a viable candidate for Gen3 CSP operating at a temperature ~750°C.

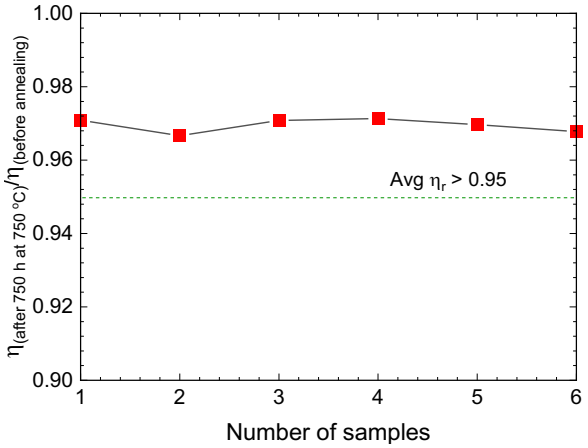

Figure 9: Efficiency ratio after to before annealing at 750°C at 750 hours 6 replicas of m-CNO coatings.

After undergoing 750 hours of isothermal heat treatment at 750 °C, the m-CNO coatings were tested for mechanical integrity, water immersion, high-temperature quenching endurance, and sand abrasion resistance. All coatings demonstrated very high endurance in these tests after the isothermal test, with an absorber efficiency ratio of greater than 0.95 before and after the test.

C.3. Diurnal Thermal Cyclic Endurance Test of m-CNO Coatings in air ST-3.3, ST-3.4, M(ST-3.4)

To determine the durability of m-CNO coating during the actual working conditions, we performed 50 cyclic day (12 hours) and night (12 hours) thermal endurance tests. Six m-CNO samples with an efficiency > 93% were prepared and heated at 750 °C for 12 hours; after that, they were kept

cool for the next 12 hours constituting one thermal cycle. Each of the six replicates was subject to 50 such thermal cycles. Optical properties—absorptance and emittance—were measured at the end of each cycle. The surface morphology and structural changes were recorded at the beginning (0^{th}), 13^{th} and 50^{th} cycles. after 50 cycles of a thermal endurance test, the average thermal emittance, of six samples remained almost equal to the initial average emittance. Absorptance also decreased at the initial stage after a few annealing cycles at 750 °C, and then remained stable. Due to the decrease in the absorptance, the coatings' efficiency also decreased at the initial stage, and then the rate of decrease was very low. The efficiency of m-CNO after 50 cycles of day and night cyclic testing was 92%.

The ratio of efficiency after 50 cycles of day-night thermal cyclic test at 750 °C to the efficiency before heat treatment of m-CNO coatings is given Figure 10. ***The average ratio of the absorber efficiency before and after the cyclic annealing test at 750 °C for 50 cycles of the six m-CNO sample was 0.97***. This value is more than our postulated absorber efficiency ratio of 0.95 for the coating heated at 750 °C for 750 hours. Therefore, we can infer that m-CNO coating is a viable candidate for the CSP operating at a temperature ~750 °C.

After undergoing 50 day-night annealing cycles at 750 °C, the m-CNO coatings were tested for mechanical integrity, water immersion, high-temperature quenching endurance, and sand abrasion resistance. All coatings demonstrated very high endurance in these tests after the 50-cycle thermal cyclic testing, with an absorber efficiency ratio of greater than 0.95 before and after the test.

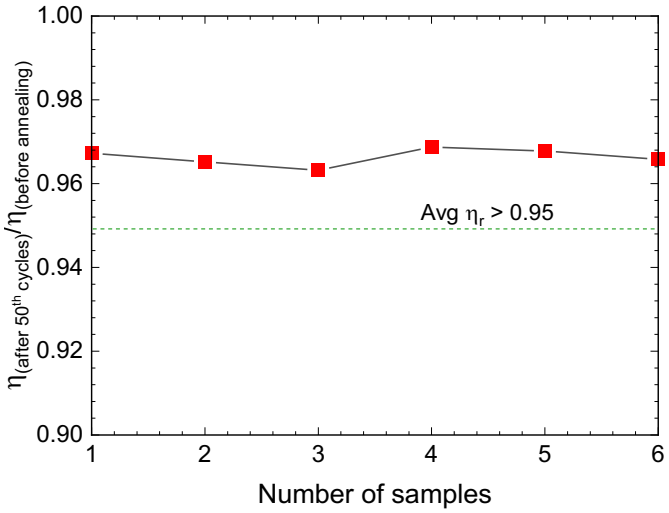

Figure 10: Efficiency ratio after to before thermal cyclic test at 750°C for 50 cycles of 6 replicas of m-CNO coatings.

D. Fabrication and Characterization of Solar Absorber Coatings on Tubular Geometry ST-6.1, ST-6.2, M(ST-6)

To achieve similar optical properties and uniformity of the absorber coating on a tubular surface as those on flat substrates by electrodeposition, we modified the experimental setup and deposited optimized m-CNO coatings of different sizes and materials on cylindrical surfaces and then evaluated the absorption with UV-Vis-NIR spectrophotometer and the morphology with a FESEM. We studied the effect of placement of reference electrode with respect to the counter electrode, keeping the working electrode fixed.

Figure 11(a-c) show the FESEM images of m-CNO coating on a cylinder at different magnifications, and Figure 11(d) displays the photograph of an m-CNO coated Inconel 625 cylinder. Figure 11(d-f) present the FESEM images of m-CNO coating on a flat substrate at different magnifications, and Figure 11(h) shows the photograph of a coating on a flat Inconel 625 substrate.

From the Field Emission Scanning Electron Microscope (FESEM) images of m-CNO coatings deposited on cylindrical substrates, it is clear that our modified deposition technique successfully enables the deposition of m-CNO coatings on cylindrical surfaces with high absorption and great uniformity.

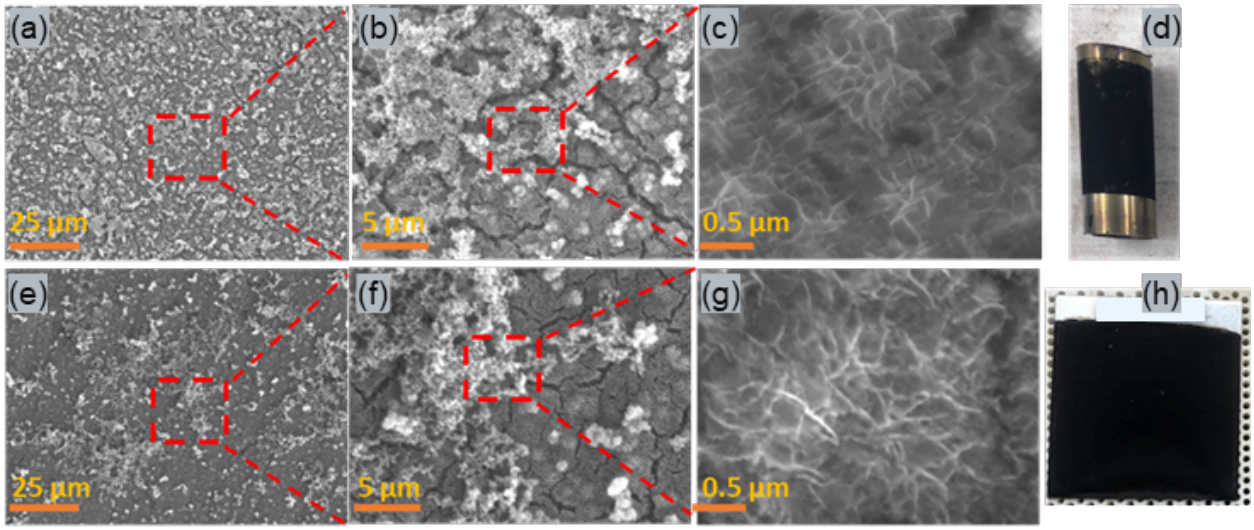

Figure 11: FESEM images of m-CNO coating at different magnifications deposited on (a-c) cylindrical surface (e-g) flat substrate. Photographs of m-CNO coated on (d) cylinder (h) flat substrates.

E. Optical and Mechanical Characterization of Absorber Coatings on Tubes M(7.1), M(7.2)

We further measured the spectral absorption of all five samples in Figure 12(a) and calculated the average absorptance as given in Figure 12(b), respectively. The results show that all the samples have an average absorptance of about 0.985, that greatly exceeds the target absorptance of 0.975.

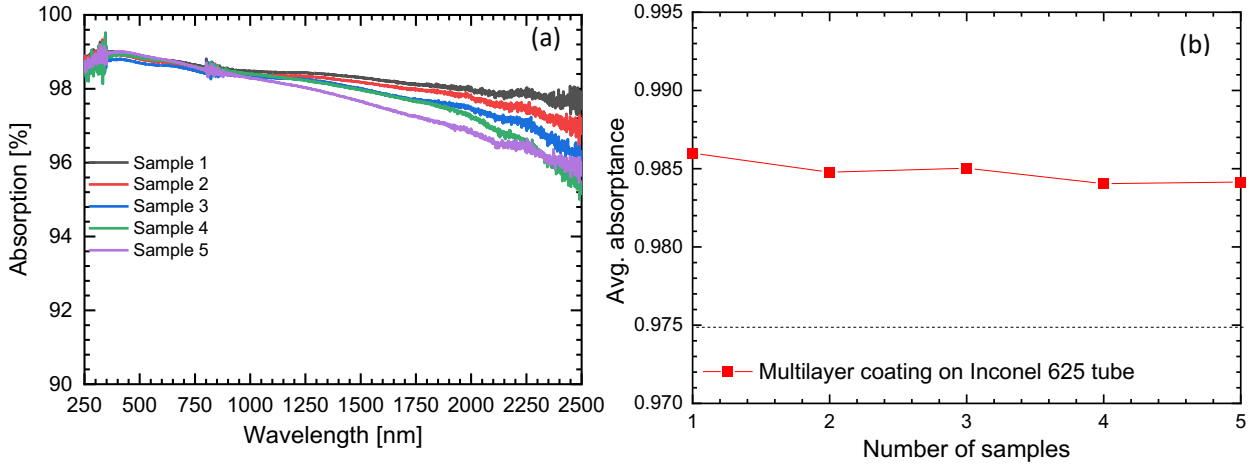

Figure 12: (a) Specular absorption spectra and (b) average absorptance of five replicates of m-CNO samples deposited on Inconel 625 cylindrical surfaces.

All five coatings underwent adhesion, water immersion, and sand abrasion tests and were found to be very robust. The optical property ratio after the tests, compared to before, was almost equal to 1, which is above the milestone target of 0.95.

F. Thermal Endurance Characterization of Absorber Coatings on Tubes M(8.1), M(8.2), M(8.3), M(8.4)

F.1. Isothermal Testing of m-CNO Coated Tubes at 750 °C for 100 and 1000 hours in Air ST-8.1, ST-8.2, M(8.1)

Five replicas of m-CNO coated cylindrical surfaces were subjected to isothermal heat treatment at 750 °C for 1000 hours in an air furnace. The spectral absorptance of five samples was recorded before and after 12, 100, 200, 500 and 1000 hours during isothermal test, and the average absorptance was calculated from these spectra. Following 100 hours and 1000 hours of isothermal heat treatment, the coatings were tested for water immersion, quenching, and adhesion endurance. The spectral absorptance of five samples was recorded before and after the isothermal tests, and the average absorptances were calculated from these spectra. The major decrease in the solar absorptance happened within the first 12 hours of heat treatment. After that the absorptance value remained nearly the same such that even after 1000 hours of heat treatment at 750°C. The absorptance ratio after to before isothermal testing was found to be greater than 0.97 for all the cases which is greater than the milestone target of 0.95. After 1000 hours isothermal test coatings are tested for the adhesion, water immersion, water quenching and sand abrasion tests which demonstrates the coating has showed the efficiency ratio before and after endurance tests were surpassed the mile stone target 0.95.

F.5. Diurnal Thermal Cyclic Testing of m-CNO Coated Tubes at 750 °C in Air ST-8.3, ST-8.4, M(8.4)

We have also examined the endurance of m-CNO coatings on cylindrical samples under day and night thermal cycling at 750°C. For that, a new set of five samples was heated at 750 °C for 12 hours and left cool for the next 12 hours. The optical properties and mechanical properties of black absorbers were recorded before the cyclic thermal test and after each step of 10 cycles of heat treatment at 750°C. Absorptance was measured both prior to and following each cycle of the cyclic test. Notably, the most significant reduction in solar absorptance occurred within the initial 10 cycles of heat treatment. Subsequently, the absorptance value remained relatively constant. Even after subjecting the coatings to 50 cycles of day and night heat treatment at 750°C, the spectral absorptance only experienced a marginal decrease of less than 2 to 3 percentage points. The absorptance ratio after 50 cycles compared to before starting cyclic testing was consistently found to be greater than **0.97** for all cases, surpassing the milestone target of **0.95**. After cyclic test coatings are tested for the adhesion, water immersion, water quenching and sand abrasion tests which demonstrates the coating has showed the efficiency ratio before and after endurance tests were surpassed the mile stone target 0.95.

G. Technoeconomic Analysis and Tech to Market Plan FD-1, FD-2

G.1. Technoeconomic Analysis

In this task, a cost/system performance model of central tubular receivers with multiscale fractal solar selective coatings was developed to compare its benefit against state-of-the-art Pyromark coating. The analysis focuses on thermal performance characteristics of external tubular solar receiver configuration with a ternary chloride salt heat transfer fluid (HTF) operating at fluid temperatures between 500–735 °C, relevant for integration with sCO_2 power cycle [7]. The cost benefit of fractal solar selective coatings (SSC) on the irradiated tubes of receiver was quantified using levelized cost of energy (LCOE) metric. The LCOE metric focuses on the cost aspects of the heliostat and receiver

sub-systems that constitute the primary components for solar to thermal energy conversion in a concentrated solar thermal (CST) plant. LCOE is defined as the lifetime cost of heliostat-receiver system that includes both the initial capital expenses and recurring coating reapplication cost to the net thermal energy absorbed by the receiver. **Fractal textured solar absorber coatings are seen to reduce LCOC by ~50% to ~67% compared to Pyromark in the actual plant conditions.**

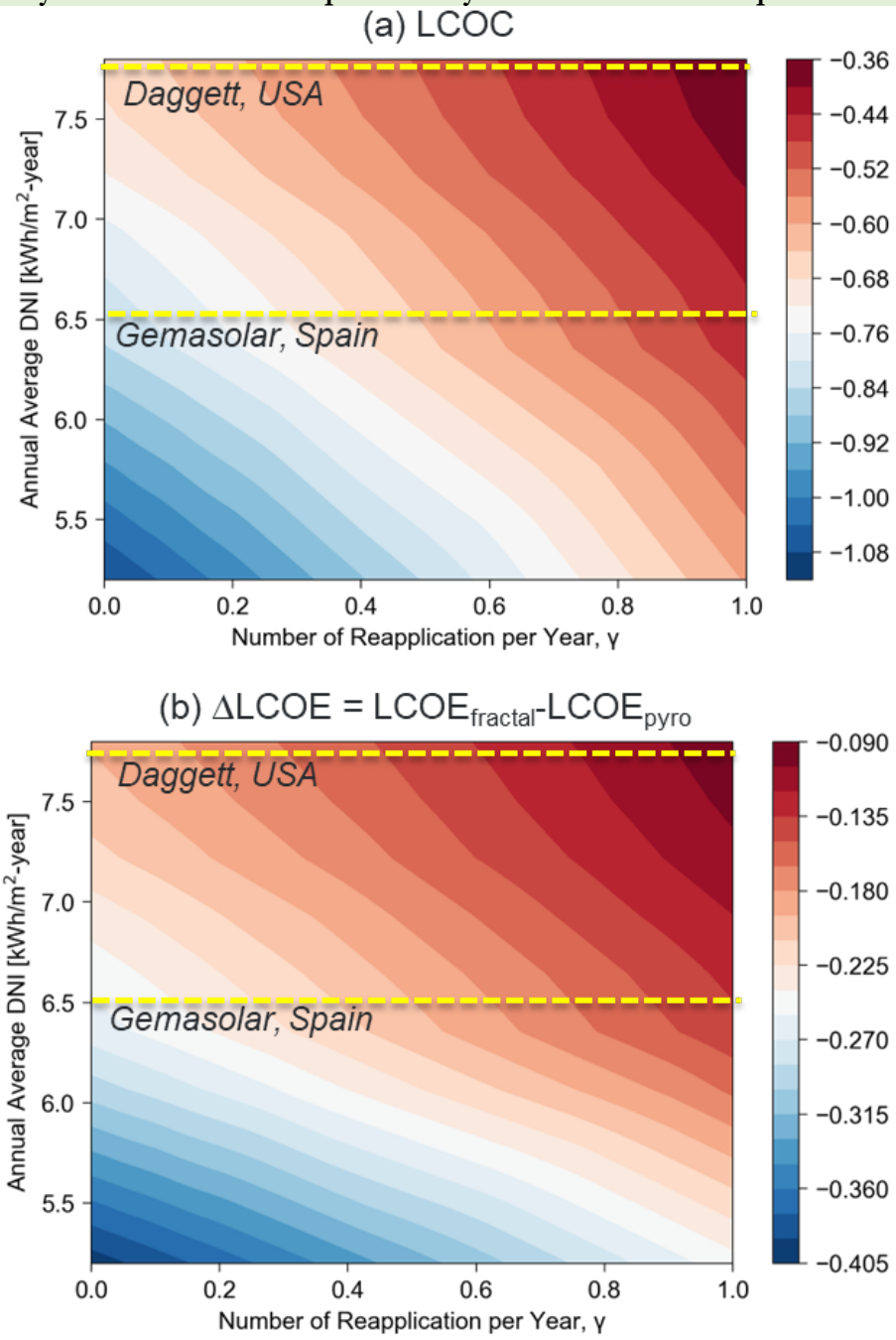

Figure 13: Contours of (a) absolute levelized cost of coating and (b) difference in LCOE between fractal SSC and state-of-the-art Pyromark as a function of annual average DNI representing different locations and number of coating reapplication per year.

Figure 13 presents contours of LCOC for the electrodeposited multiscale CoNiO coating and difference in LCOE between fractal SSC and state-of-the-art Pyromark denoted by ΔLCOE. This

visualization is presented as a function of the annual average Direct Normal Irradiance (DNI) and the number of coating reapplications per year. **The contour plot provides a comprehensive overview, showing how the economic considerations represented by LCOC and ΔLCOE vary across different locations and coating maintenance scenarios. The negative LCOC and ΔLCOE values underscores the techno-economic competitiveness of multiscale CoNiO coating. The sensitivity to DNI variations highlights the significance of selecting coatings that can maximize energy absorption in regions with lower solar irradiance (ΔLCOE is larger at locations with lower DNI), ensuring the economic viability and efficiency of CST systems across diverse geographical locations.**

G.2. Tech to Market Plan

A patent application has been filed through the Virginia Tech Intellectual Properties office based on the invention developed in this project. For industry acceptance of the technology, detailed on-sun testing studies are being pursued as part of the NREL Optical Materials Characterization Laboratory.

H. Summary and Conclusions

Based on the studies, the following principal summary points are drawn, grouped by the major tasks of the project:

Coating Fabrication and Durability

1. A statistically designed experiment matrix of fabrication parameters, substrates, substrate texturing and coatings was developed based on a comprehensive literature review.
2. Highly textured multiscale surfaces composed of single and multiple layers were deposited on various substrate materials of flat and cylindrical geometry.
3. Fractal dimension greater than 1.5 and up to 1.9 was demonstrated for replicates of different black absorber with efficiency >93%.
4. Electrodeposition conditions, coating materials, substrate materials, substrate finishes were optimized to achieve **highest ever absorber efficiency of up to 95.52%** that surpassed the project milestone of 93%.
5. Adhesion test and water immersion endurance test for coatings deposited by electrodeposition were conducted to demonstrate that those coatings have excellent endurance in all conditions with absorber efficiency after durability testing/before durability testing > 0.95 by one-tailed Student t-test with up to 99% confidence level.
6. Mechanical abrasion test on electrodeposited surfaces showed that the coatings were mechanically stable under harsh SiC grain impingement. The coatings were shown to have efficiency ratio > 0.95 for over 90g and up to 400g of grain flow. These were shown to be quite aggressive compared to conditions that the receiver coating may endure in a 30-year service lifetime.

Thermal Endurance and Thermal Cyclic Testing

7. Replicates of single and multilayer absorber coatings were prepared on Inconel 625 substrates and subject to isothermal and thermal cycling endurance testing at 750°C for up to 1000 h and 50 diurnal temperature cycles.
8. Multilayer fractal textured cobalt-nickel coatings were shown to be an attractive candidate for Gen3 solar tower application. The coatings demonstrated impressive as fabricated **absorptance an efficiency of 95.38%**.

9. Iron containing metal oxides deposited by electrodeposition showed lower absorber efficiency than those needed for the high-temperature application.
10. Multilayer fractal textured CoNiO coatings showed the best **high-temperature endurance** among all the black absorber coatings. For coatings on tubular sections, the absorptance ratio after 1000 h of isothermal exposure at 750°C to before the isothermal endurance test stayed above 0.97, which exceeds the aggressive target (0.95) of the project.
11. Multilayer fractal textured CoNiO coatings showed the best **thermal cyclic endurance** among all the black absorber coatings. For coatings on tubular sections, the absorptance ratio after 50 cycles of diurnal cycling at 750°C to before the cycling test stayed above 0.97, which exceeds the aggressive target (0.95) of the project. The absorber efficiency was above 93.1% after the 50 cycles, well above the SETO target of > 90% efficiency.
12. Optical and morphological studies established that changes in the optical properties and morphology of the black absorber coatings happened within the first 12 hours of heating at 750 °C in both isothermal and thermal cyclic endurance tests. After that, optical properties and morphologies were stable for over 1000 hours and over 50 cycles.

Coating Durability After Isothermal and Thermal Cyclic Endurance Testing

13. After isothermal annealing for 1000 hours at 750°C and 50 diurnal cycling up to 750°C, the adhesion test, high-temperature water quenching test, and water immersion test on m-CNO coating indicated outstanding durability in all tests with no loss of absorber efficiency. The ratio of the optical properties after testing to before testing was near 1.0 exceeding the milestone target value of 0.95.
14. Falling sand abrasion testing of the coatings that underwent 1000 h isothermal endurance and 50 cycle thermal cyclic testing at 750°C demonstrated that the coatings FOM ratio was about 0.98, far exceeding the milestone target of 0.95 for over 60 g of sand impingement, which corresponds to the conditions of a harsh desert environment over 30 years.

Technoeconomic Analysis

15. The fractal textured CoNiO coatings are shown to have lower LCOC of $-0.007/MWht at the higher temperature of 750 °C relative to the benchmark LCOC of Pyromark ($0.055/MWht) at a more benign, lower temperature of 700 °C, thereby exceeding the SOPO EOP-C target.
16. The fractal textured solar absorber coatings are seen to reduce LCOC by ~50% to ~67% compared to Pyromark in the actual plant conditions.
17. The negative LCOC and ΔLCOE values underscores the techno-economic competitiveness of multiscale CoNiO coating.

Overall, the project demonstrated the excellent performance and cost-effectiveness of the developed novel fractal textured solar absorber coatings for Gen3 CSP applications. The coatings featured the highest ever absorptance, a low emittance and an overall high absorber efficiency at 750°C, with exceptional thermal and mechanical durability.

	Metric	Success Value	Assessment tool	Measured value	Goal Met (Y/N)
Milestone 1.1	Design of Experiments	Development of experimental design matrix which incorporates all the factors including choice of substrate, coating material and electrodeposition process conditions.			Y
Milestone 1.3	SSC Fractal Characterization	Fractal dimension > 1.5, of which at least 10 replicates for each combination identified in the design of experiment matrix are suitable for FOM testing.	One tailed Student t-test at 95% confidence level	Electrodeposited CuMnO CuCoO coatings on Inconel 625 substrate showed fractal dimension >1.8	Y
Milestone 2.1	Optical characterization: Optical properties of the samples namely, solar absorptance and thermal emittance of the prepared samples will be measured to calculate the figure of merit	Demonstrate FOM > 0.93 at concentration ratio of 1000 suns and temperature of 750°C demonstrated at least on ten replicates that will be used for isothermal and thermal cycling endurance testing.	One-tailed Student t-test at 95% confidence level FOM measured mean > FOM success value	CuMnO showed mean absorptance 0.980 and emittance 0.395. CuCoO showed mean absorptance 0.978 and emittance 0.398. Mean absorber efficiency of CuMnO, 95.52% and CuCoO, 95.35% > efficiency success value, 93%.	Y Y
G/NG-1	Mechanical durability testing using the ASTM protocols	Demonstrate FOM > 0.93, Adhesion strength > 0.95, Mechanical durability endurance> 0.95, and Water durability endurance > 0.95 for at least 10 replicates that will be used for isothermal and thermal cycling endurance testing.	One-tailed Student t-test at 95% confidence level FOM measured	1) Electrodeposited CuMnO and CuCoO showed FOM > 93% 2) Ratio of absorber efficiency before	Y Y

			mean > FOM success value	adhesion test over after adhesion test was> 0.99, (success vale 0.95) 3) Ratio of absorber efficiency after and before water endurance test of CuMnO and CuCoO was > 0.99 (Success value 0.95) 4) Destructive sand abrasion test showed CuMnO could withstand more than 400g of SiC mass with absorber efficiency ratio > 0.95. CuCoO can withstand 90g of SiC mass with an absorber efficiency ratio.	Y Y
Milestone ST-3.2	Isothermal Endurance testing at 750 °C for 100 h	1. Isothermal endurance: FOM [t=100h,750 C]/FOM [t=0h,750 C]> 0.98; 2. Adhesion strength based on ASTM D3359: FOM after adhesion testing [t=100h,750 C]/FOM before adhesion testing [t=100h,750 C] > 0.95; 3. Mechanical durability endurance: FOM after durability testing [t=100h,750 C]/FOM before durability testing [t=100h,750 C] > 0.95; 4. Water durability endurance: FOM after durability testing [t=100h,750 C]/FOM before durability testing [t=100h,750 C] > 0.95;	Figure of merit for t = 100h and T = 750 C calculated. One-tailed Student t-test at 95% confidence level	(1) Mean absorber efficiency ratio > 0.98 (**meets target milestone 0.98**) (2–4) Mean absorber efficiency ratio = 1 (**exceeds target of 0.95**)	Y

		5. Water Quenching endurance: FOM before quenching [t=100h,750 C]/FOM after quenching [t=100h,750 C] > 0.95			
Milestone ST-3.3	Isothermal Endurance testing at 750 °C for 750 h	1. Isothermal endurance: FOM [t=100h,750 C]/FOM [t=0h,750 C] > 0.95; 2. Adhesion strength based on ASTM D3359: FOM after adhesion testing [t=100h,750 C]/FOM before adhesion testing [t=100h,750 C] > 0.95; 3. Mechanical durability endurance: FOM after durability testing [t=100h,750 C]/FOM before durability testing [t=100h,750 C] > 0.95; 4. Water durability endurance: FOM after durability testing [t=100h,750 C]/FOM before durability testing [t=100h,750 C] > 0.95; 5. Water Quenching endurance: FOM before quenching [t=100h,750 C]/FOM after quenching [t=100h,750 C] > 0.95	Figure of merit for t = 100h and T = 750 C calculated. One-tailed Student t-test at 95% confidence level	(1) Mean absorber efficiency ratio =0.97 (**exceeds target milestone 0.95**) (2–4) Mean absorber efficiency ratio = 1 (**exceeds target of 0.95**)	Y
Milestone ST-3.4	Thermal cyclic testing of the samples at 750 °C for 50 cycles	1. Thermal Cycling endurance = FOM [50 cylces,750 C]/ FOM [t=0h,750 C] > 0.95; 2. Adhesion strength based on ASTM D3359: FOM after adhesion testing [t=100h,750 C]/FOM before adhesion testing [t=100h,750 C] > 0.95; 3. Mechanical durability endurance: FOM after durability testing [50 cylces,750 C]/ FOM before durability testing [50 cylces,750 C] > 0.95; 4. Water durability endurance: FOM after durability testing [50 cylces,750 C]/FOM before durability testing [50 cylces,750 C] > 0.95; 5. Water Quenching endurance: FOM before quenching [50 cylces,750 C]/FOM after quenching [50 cylces,750 C] > 0.95	Figure of merit for t = 100h and T = 750 C calculated. One-tailed Student t-test at 95% confidence level	(1) Mean absorber efficiency ratio =0.97 (**exceeds target milestone 0.95**) (2–4) Mean absorber efficiency ratio = 1 (**exceeds target of 0.95**)	Y

Milestone ST-6	Fabrication and Characterization of Solar absorber coatings on tubes	Comparable morphology and fractal development on tubular surfaces compared to coatings for flat surfaces.	Fractal dimension		
Milestone M(7.1)		Demonstrate absorptance > 0.975 for 5 samples of SAC coating on the tubular surfaces. By comparing the optical characteristics, demonstrate that cylindrical surfaces have homogeneous coatings throughout the four quadrants and length of the tubes.	Absorptance		
Milestone M(7.2)		Demonstrate absorptance > 0.975, Adhesion strength > 0.95, Mechanical durability endurance> 0.95, and Water durability endurance > 0.95 for at least 10 replicates that will be used for isothermal and thermal cycling endurance testing.	Absorptance, Adhesion Strength, Mechanical durability endurance based on sand abrasion ASTM D968, Water durability endurance based on ASTM D870		
Milestone M(8.1) 100h		Demonstrate 1. Isothermal endurance = Absorptance [t=100h,750 C]/ absorptance [t=0h,750 C] >0.95 2. Adhesion strength = Absorptance after adhesion test [t=100h,750 C]/ absorptance before adhesion test [t=100h,750 C] > 0.95, 3. Mechanical durability endurance: absorptance after durability testing [t=100h,750 C]/ absorptance before durability testing [t=100h,750 C] > 0.95 4. Water durability endurance: absorptance after durability testing [t=100h,750 C]/absorptance	at 750 C <u>for 100 hours</u> Adhesion measure Mechanical durability endurance based on sand abrasion ASTM D968 Water durability endurance based on ASTM D870		

		before durability testing [t=100h,750 C] > 0.95 5. Water Quenching endurance: absorptance after quenching [t=100h,750 C]/absorptance before quenching [t=100h,750 C] > 0.95	Water Quenching test from 750 C		
Milestone M(8.2) 1000h		Demonstrate 1. Isothermal endurance = Absorptance [t=1000h,750 C]/ absorptance [t=0h,750 C] >0.95 2. Adhesion strength = Absorptance after adhesion test [t=1000h,750 C]/ absorptance before adhesion test [t=1000h,750 C] > 0.95, 3. Mechanical durability endurance: absorptance after durability testing [t=1000h,750 C]/ absorptance before durability testing [t=1000h,750 C] > 0.95 4. Water durability endurance: absorptance after durability testing [t=1000h,750 C]/absorptance before durability testing [t=1000h,750 C] > 0.95 5. Water Quenching endurance: absorptance after quenching [t=1000h,750 C]/absorptance before quenching [t=1000h,750 C] > 0.95	Isothermal endurance at 750 C <u>for 1000 hours</u> Adhesion measure Mechanical durability endurance based on sand abrasion ASTM D968 Water durability endurance based on ASTM D870 Water Quenching test from 750 C		
Milestone M(8.3) 10 cycles		Demonstrate: 1. Thermal Cycling endurance = Absorptance [10 cycles,750 C]/ absorptance [t=0h,750 C] >0.95 2. Adhesion strength = Absorptance after adhesion test [10 cylces,750 C]/ absorptance before adhesion test [10 cycles,750 C] > 0.95, 3. Mechanical durability endurance: Absorptance after durability testing [10 cycles,750 C]/ absorptance before durability testing [10 cycles,750 C] > 0.95 4. Water durability endurance: Absorptance after durability testing [10 cycles,750 C]/absorptance before durability testing [10 cycles,750 C] > 0.95 5. Water Quenching endurance: Absorptance	Thermal Cycling endurance at 750 C <u>for 10 cylces</u> Adhesion measure Mechanical durability endurance based on sand abrasion ASTM D968 Water durability endurance based on ASTM D870		

		after quenching [10 cycles,750 C]/absorptance before quenching [10 cycles,750 C] > 0.95	Water Quenching test from 750 C		
Milestone M(8.4) 50 cycles		Demonstrate: 1. Thermal Cycling endurance = Absorptance [50 cycles,750 C]/ absorptance [t=0h,750 C] >0.95 2. Adhesion strength = Absorptance after+D50+D56	Thermal Cycling endurance at 750 C <u>for 50 cylces</u> Thermal Cycling endurance Adhesion measure Mechanical durability endurance based on sand abrasion ASTM D968 Water durability endurance based on ASTM D870 Water Quenching test from 750 C		
EOP-C		Identify successful coating, process parameter and receiver design that demonstrate LCOC < 0.055$/MWht at 750°C (LCOC for Pyromark 2500 at 565℃)	Levelized Cost of Coating (LCOC)	LCOC of $–0.007/MWht < $0.055/MWht for Pyromark	Y

Impact[2]:

The underlying scientific novelty of this project is that of generating multiscale surface topologies on metallic surfaces by tailoring the operating parameters of the industrially widely used electrodeposition process. The generated multiscale fractal surface textures would provide for exceptionally high light trapping without losing the energy to the ambient, which forms the basis of the desired high collection efficiency. Since the process applies across metallic materials, it can be used to fabricate a large area solar selective surface on high temperature materials cost-effectively, leading to low levelized coating cost.

This research addresses the overall DOE SETO mission to support early-stage research and development to improve the performance and flexibility of solar technologies that contribute to a reliable and resilient U.S. electric grid. Specifically, the project is focused on supporting advanced innovation in Advanced CSP Thermal Transport System and Components. The developed coating enables achieving > 90% receiver thermal efficiency for next gen CSP plants operating at temperature > 750°C. Successful demonstration of the novel cost-effective coatings that maintain high absorptivity while minimizing emissivity and maintain prolonged stability at high temperatures in air (>750°C) paves the way for deployment of advanced, high temperature and high efficiency power cycles, reduction in receiver cost and solar field cost (reduction in number of heliostats), due to improved thermal efficiency. Operation at high temperatures also brings down the thermal storage cost due to high energy storage capacity. The combined benefits will enable achieving DOE SETO receiver cost target of <150$/kW.

Overall, the project demonstrated the excellent performance and cost-effectiveness of the developed novel fractal textured solar absorber coatings for Gen3 CSP applications. The coatings featured the highest ever absorptance, a low emittance and an overall high absorber efficiency at 750°C, with exceptional thermal and mechanical durability.

Changes/Problems[3]:

Products[4]:

The following publications resulted from the work presented in this report:

1. K. Kant, K.P. Sibin and R. Pitchumani, "Novel Fractal-textured Solar Absorber Surfaces for Concentrated Solar Power," *Solar Energy Materials and Solar Cells*, 248, 112010, 2022. https://doi.org/10.1016/j.solmat.2022.112010.
2. K.P. Sibin, K. Kant, and R. Pitchumani, "High-Temperature Air Stability of Electrodeposited Copper Cobalt Oxide and Copper Manganese Oxide Absorber Coatings for Concentrating Solar Power," *ACS Applied Energy Materials*, **6**(17), 8759–8774, 2023. https://doi.org/10.1021/acsaem.3c01224.
3. K.P. Sibin and R. Pitchumani, "Multiscale Textured Air Stable Solar Absorber Coatings for Next-Generation Concentrating Solar Power," *Renewable and Sustainable Energy Reviews*, In Review, 2024.
4. R. Pitchumani and S.K. Purayil, Fractal Textured High Efficiency Solar Absorber Coatings, U.S. Provisional Patent No. 63/329,842, PCT/US23/18223 (Patent pending).

[2] See EERE 355 FARC Section IA5
[3] See EERE 355 FARC Section IA6
[4] See EERE 355 FARC Section IA3

Participants & Collaborators[5]:

Sibin Purayil (Postdoctoral Fellow)
Karunesh Kant (Postdoctoral Fellow)
Paruchuri Kondaiah (Postdoctoral Fellow)
Karthik Nithyanandam (Consultant)
Ranga Pitchumani (Principal Investigator)

References:

[1] A. Zaleski, Fractals And The Weierstrass-Mandelbrot Function, Rose-Hulman Undergrad. Math. J. 13 (2012) 79–113.

[2] A. Brown, G. Savary, Describing ground surface texture using contact profilometry and fractal analysis, Wear. 141 (1991) 211–226.

[3] A. Majumdar, B. Bhushan, Fractal Model of Elastic-Plastic Contact Between Rough Surfaces, J. Tribol. 113/1 (1991) 1–11.

[4] F. YANG, R. PITCHUMANI, Fractal Description of Interlaminar Contact Development during Thermoplastic Composites Processing, J. OfREINFORCED Plast. Compos. 20 (2001) 536–546. https://doi.org/10.1106/DAEQ-L4HD-N45W-4MJR.

[5] K. Kant, K.P. Sibin, R. Pitchumani, Novel fractal-textured solar absorber surfaces for concentrated solar power, Sol. Energy Mater. Sol. Cells. 248 (2022) 112010. https://doi.org/10.1016/j.solmat.2022.112010.

[6] K.P. Sibin, K. Kant, R. Pitchumani, High-Temperature air stability of elctrodeposited copper cobalt oxide and copper manganese oxide absorber coatings for concentrating solar power, ACS Appl. Energy Mater. 6 (2023) 8759−8774. https://doi.org/10.1021/acsaem.3c01224.

[7] M. Mehos, C. Turchi, J. Vidal, M. Wagner, Z. Ma, C. Ho, W. Kolb, C. Andraka, A. Kruizenga, Concentrating Solar Power Gen3 Demonstration Roadmap, 2017. https://doi.org/10.2172/1338899.

[5] See EERE 355 FARC Section IA4